Computational *S*imulations of Hydrated Strontium Hydroxides

- 15th November 20161
- Olivia Lynes
- Supervisor: Andy Kerridge
- Industrial supervisor: Jonathan Austin

Talk Overview

- Aims of the project
- Previous work
- Aquo Complexes
- Hydroxide Complexes
  - Mono-hydroxide system
  - Di-hydroxide system
- Bulk Oxide- CeO2

Aim of Project

Lancaster University

Computational simulations of storage pond sludge disturbance

- Understanding the interactions of:
  - Strontium, caesium, uranium with particulates.
- *ab initio* molecular dynamics:
  - Large amount of data
  - Novel research method for this area.
- Studying:
  - Hydration Structure
  - Absorption effects/ surface interaction.
  - pH Effects.

Previous Work- Strontium Structures

- DFT gas phase and aqueous phase micro solvation.
- 3 heptahydrates
- 7 CN energetically stable.

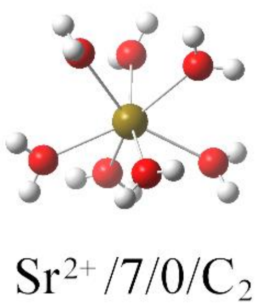

Figure 1. TPSS optimised Sr^{2+} heptahydrate.

A.Kerridge, N.Kaltsoyannis 2011
DOI:10.1002/chem.201003226

- DFT calculations of Sr^{2+} hydroxides with a continuum solvent model.
- Proton transfer mechanism.
- Energy barrier 3.0 kJ/mol

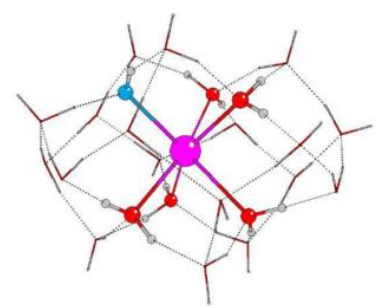

Figure 2. Sr^{2+} 5 Coordinated mono-hydroxide

E. Makkos, A.Kerridge, N.Kaltsoyannis 2015
DOI: 10.1039/C5DT01110H

Methodology

- CP2K (version 3)
  - Periodic planewave code

- *ab initio* molecular dynamic (AIMD) calculations.
  - Total simulation time of 20 picoseconds
  - 5 picosecond equilibration period
  - 0.5 fs timestep- 1/10th smallest vibration

- Gaussian Augmented Planewave method (GAPW)
  - Goedecker-Teter-Hutter (GTH) pseudopotentials

- Nosè-Hoover thermostat

Aquo Complexes

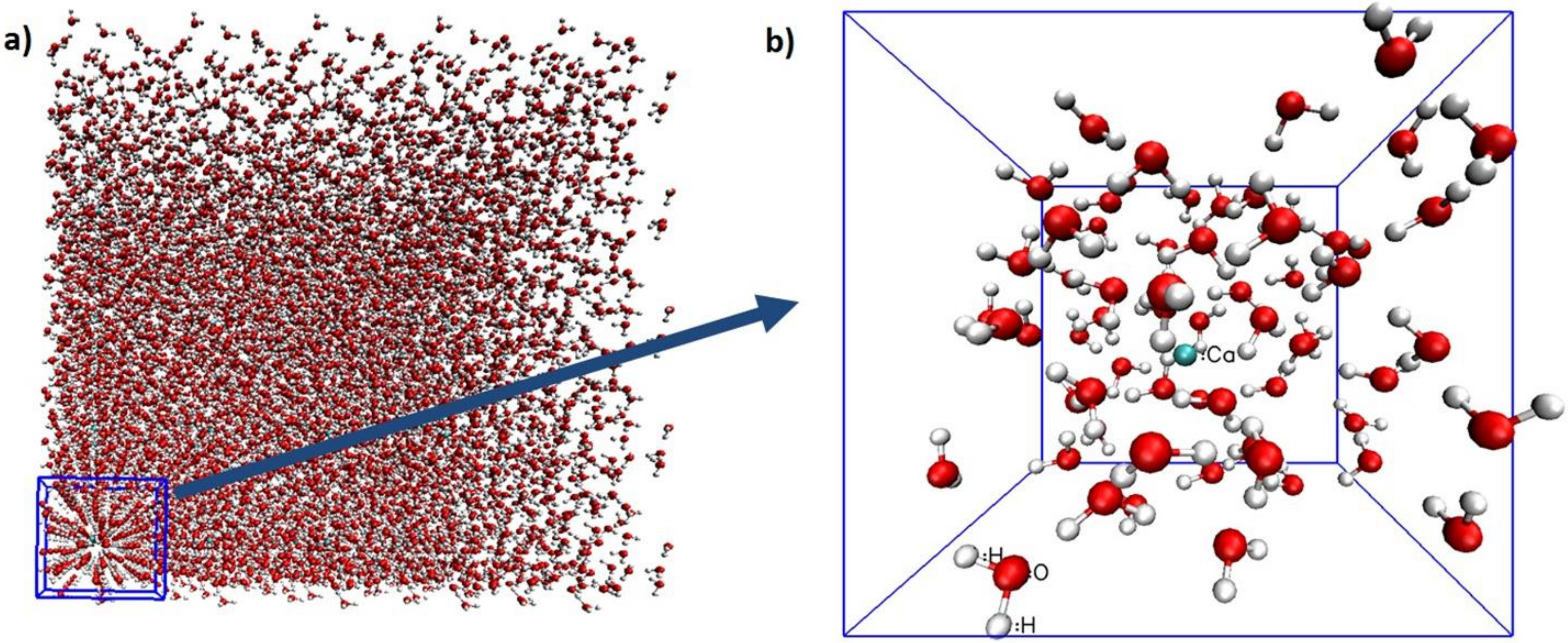

Figure 1: a) Periodic representation of the system. B) Single unit of 64 H_2O molecules with central metal ion (Ca^{2+})

- 11.99 Å box length
- N-H thermostat 400 K
- PBE/DZVP with dispersion

Aquo Complexes

Coordination Number (CN)

- Coordination of waters to the metal ion calculated at each step.
- Any CN which lasted less than 0.5 ps discounted as “not a true transition”

Bond Length

- Average bond length for the first solvation shell.

	CN Residence time %						
	6	7	8	Av. CN	Lit Value	Av. Bond Length/ Å	Lit Value/Å
Mg	100			6.00	6	2.20	2.07-2.12
Ca		43.88	56.12	7.56	6-8	2.52	2.35-2.68
Sr			100	8.00	7-9	2.66	2.52-2.69

Mono-hydroxide

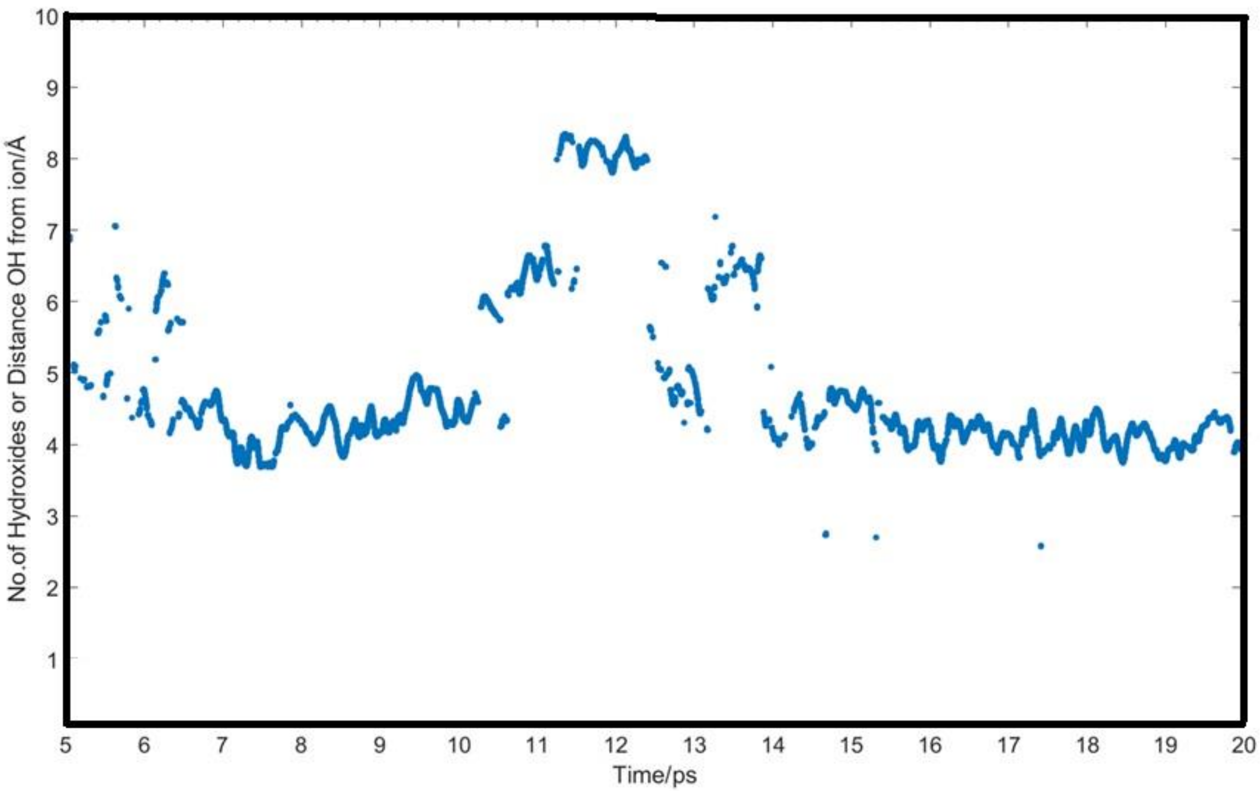

- Single hydroxide
- Initially in 1st solvation shell
- Hydroxide at a distance > 4 Å from strontium ion
- Proton transfer or proton migration?

Mono-hydroxide

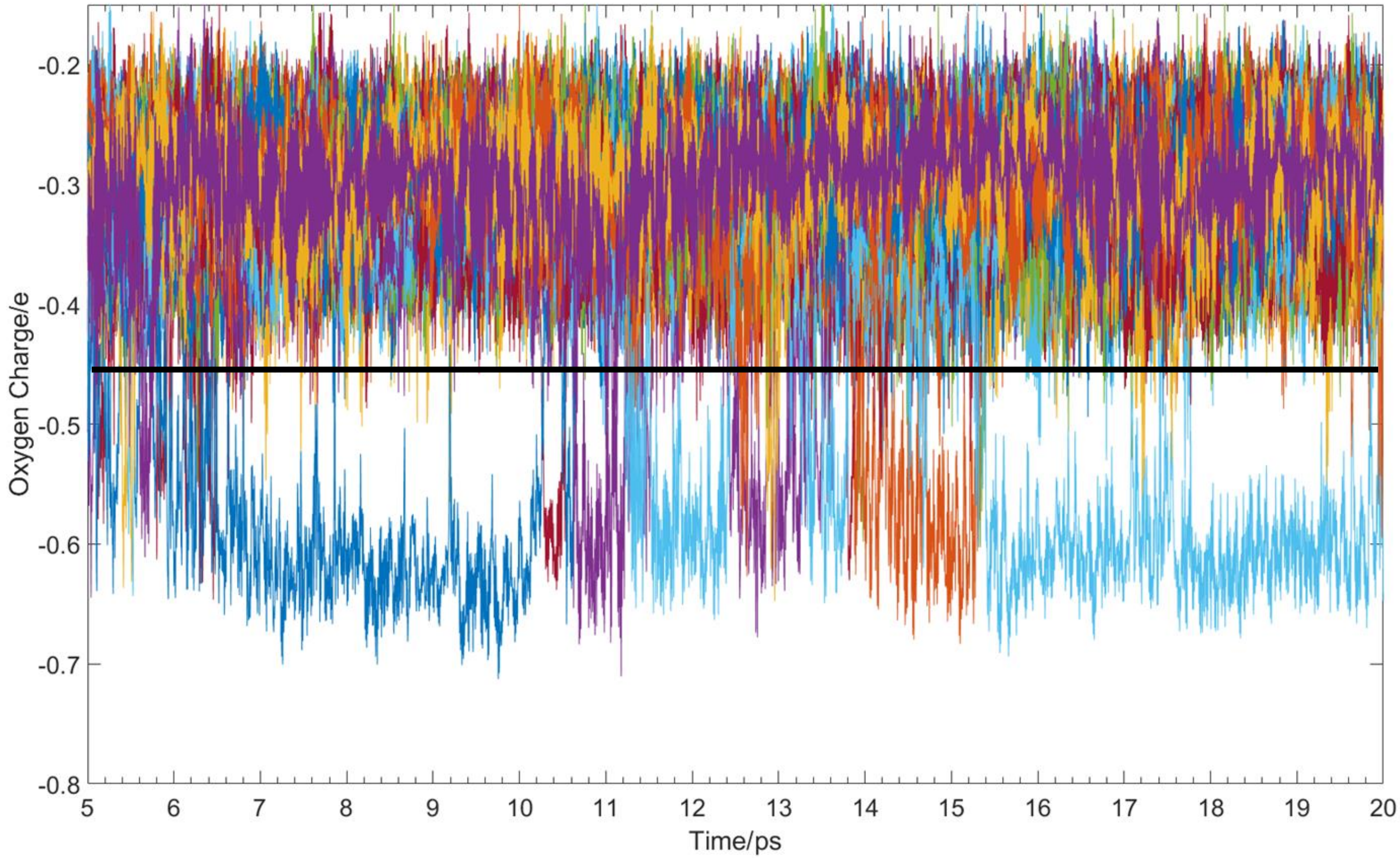

- Charge less than -0.57 cut off for hydroxide
- 19 separate oxygens considered a hydroxide across the timescale of reaction

Di-hydroxide Complexes-

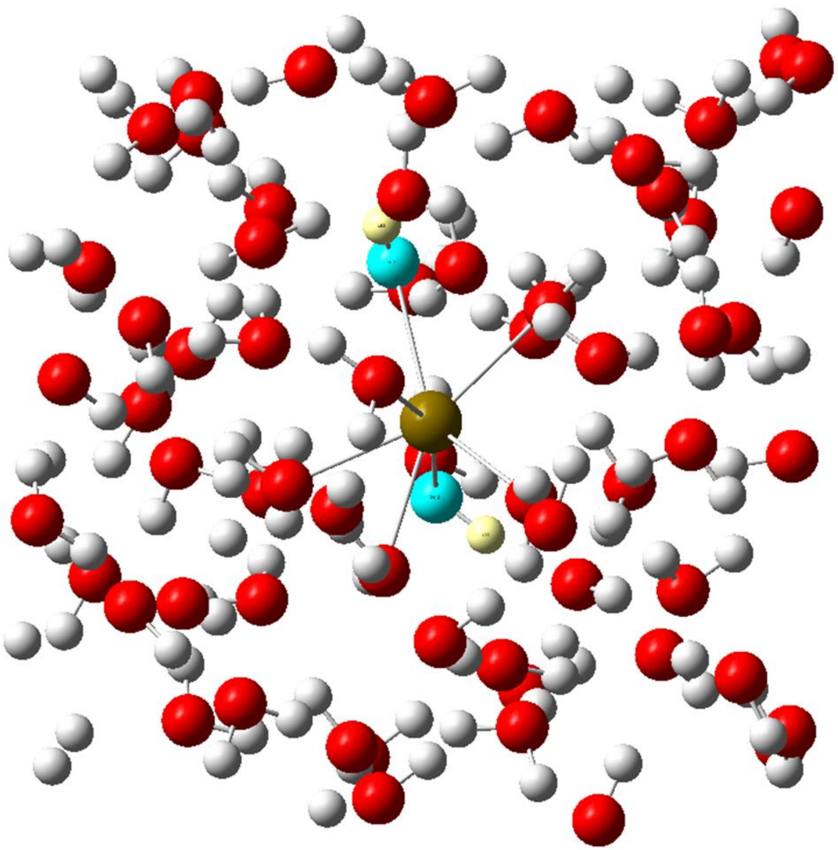

Figure 3: Visual representation of a strontium di-hydroxide. 2 OH- ions (O- blue, H- Yellow) with a Sr^{2+} ion (brown) in the centre.

Initial Di-Hydroxide Systems

Both OH^- placed at a distance > 3Å away from the metal ion.

Both OH^- placed at a distance of < 3Å from the metal ion.

One OH^- placed at a distance of < 3 Å, one placed at a distance of > 3 Å.

Di-hydroxide Average Bond Lengths

Lancaster University

OH Each Solvation Shell	Average Bond Length / Å				Average per "system type" / Å
Mg	2.16	2.17	2.13	2.20	2.17
Ca	2.59	2.48	2.46	2.52	2.51
Sr	2.73	2.63	2.63	2.70	2.67
OH first solvation shell					
Mg	2.15	2.17	2.24	TBC	2.19
Ca	2.67	2.42	2.53	2.44	2.51
Sr	2.62	2.73	2.69	2.66	2.67
OH second solvation shell					
Mg	2.23	2.15	2.14	2.09	2.15
Ca	2.58	2.57	2.52	2.47	2.54
Sr	2.67	2.74	2.64	2.66	2.68

Average Coordination Number

	Average CN				Average CN per "system"
OH in each Shell	1	2	3	4	
Mg	6.00	6.00	6.00	6.00	6.00
Ca	6.90	6.47	6.67	6.17	6.55
Sr	8.01	6.86	7.65	7.48	7.50
Both in first solvation shell					
Mg	6.00	6.00	5.70	TBC	5.90
Ca	7.07	6.16	6.54	6.60	6.59
Sr	7.00	7.45	7.64	7.50	7.40
Both in second solvation shell					
Mg	5.72	6.00	6.00	5.97	5.92
Ca	6.98	6.73	6.86	6.83	6.85
Sr	8.04	7.61	7.46	7.78	7.72

Residence Time
One OH in each Shell

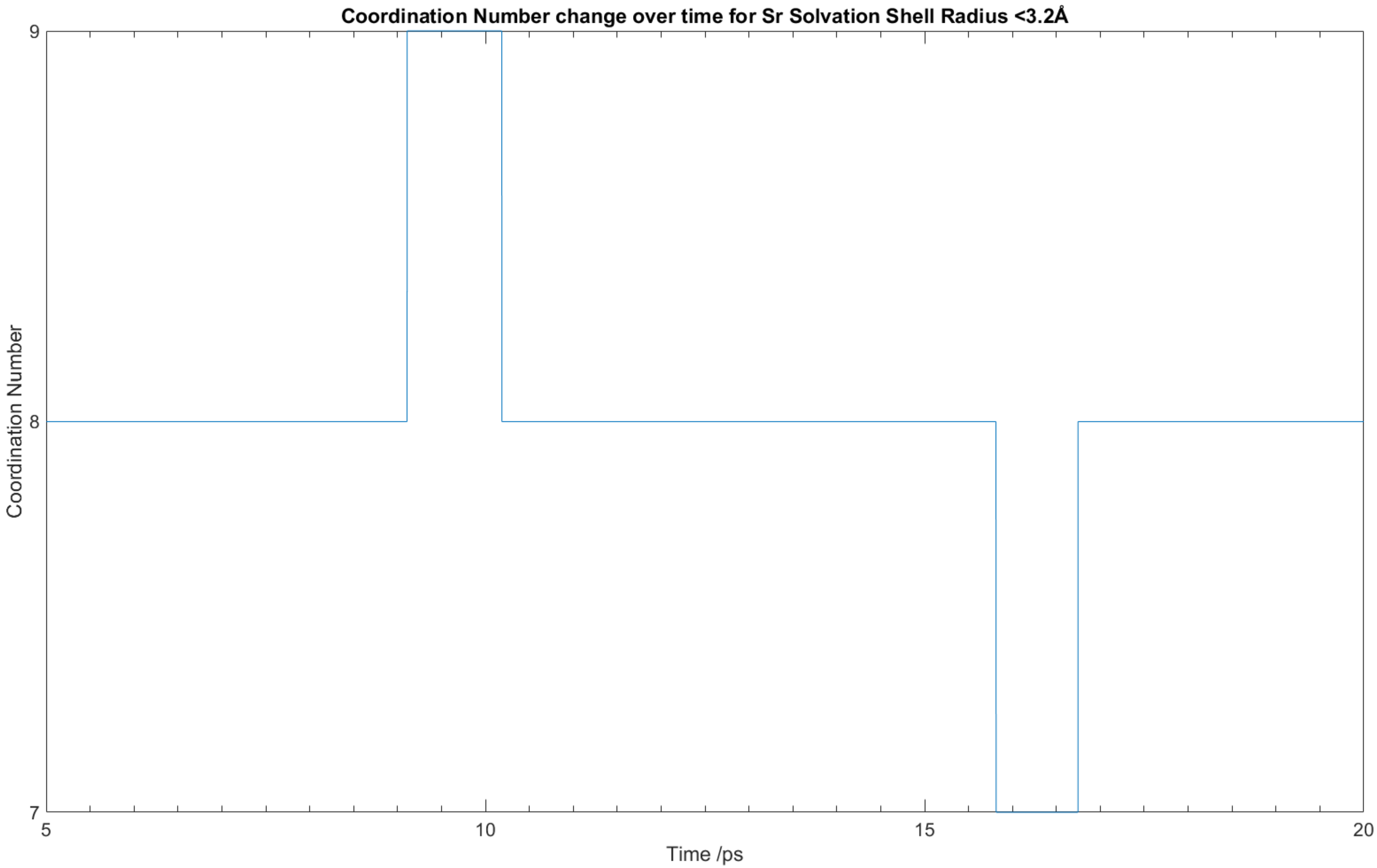

Residence Time
OH in each Shell

	% Residence Time				Average CN 2d.p
CN	**6**	**7**	**8**	**9**	
Mg	100.00	0.00	0.00	0.00	6.00
	100.00	0.00	0.00	0.00	6.00
	100.00	0.00	0.00	0.00	6.00
Ca	40.09	29.64	30.26	0.00	6.90
	61.74	29.48	8.78	0.00	6.47
	0.00	92.80	7.20	0.00	7.07
	33.41	35.56	31.03	0.00	6.98
Sr	0.00	6.22	86.59	7.19	8.01
	14.01	85.99	0.00	0.00	6.86
	0.00	36.26	63.74	0.00	7.64
	0.00	22.35	77.65	0.00	7.78

Hydroxide Summary

	Overall Average Bond Length / Å		
	Mg	Ca	Sr
Average Bond Length	2.17	2.52	2.67
Standard Deviation	0.04	0.07	0.04

	Overall Average CN		
	Mg	Ca	Sr
Coordination Number	5.94	6.66	7.54
Standard Deviation	0.11	0.28	0.33

Oxide Surface- CeO_2

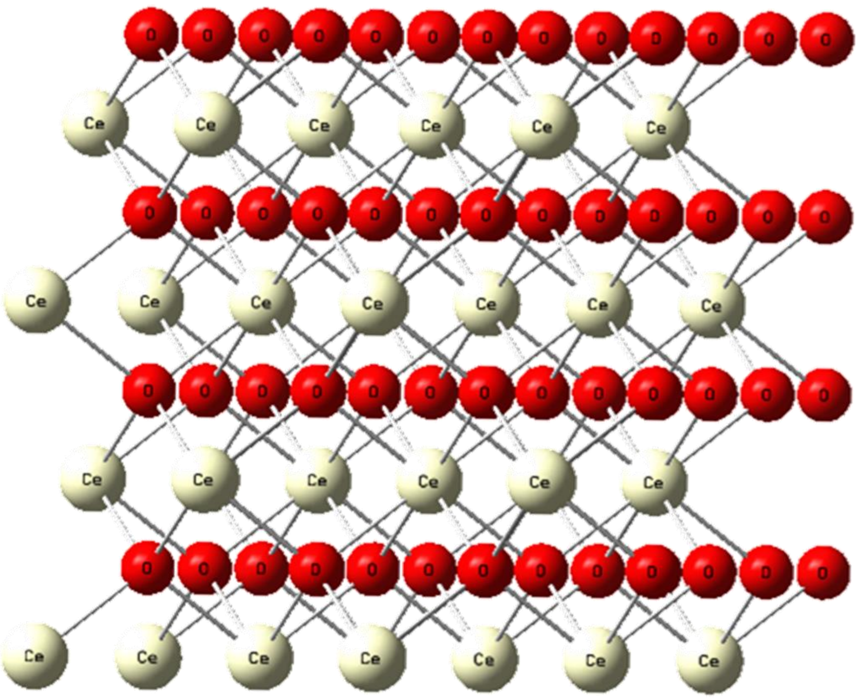

Why CeO_2?

- UO_2 is one of the main minerals of interest.
- Interested in the absorption of radionuclides onto the mineral surface.
- Uranium dioxide is not easily modelled and not currently available in CP2K.
- CeO_2 is a well known analogue for Uranium dioxide, as it closely resembles the mineral structure of fuel grade UO_2.
- It is already used both computationally and experimentally with good results.

How it all links together

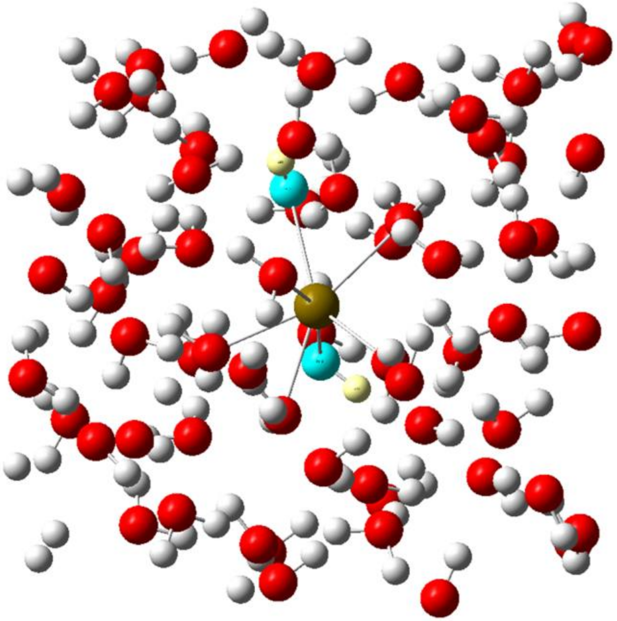

+

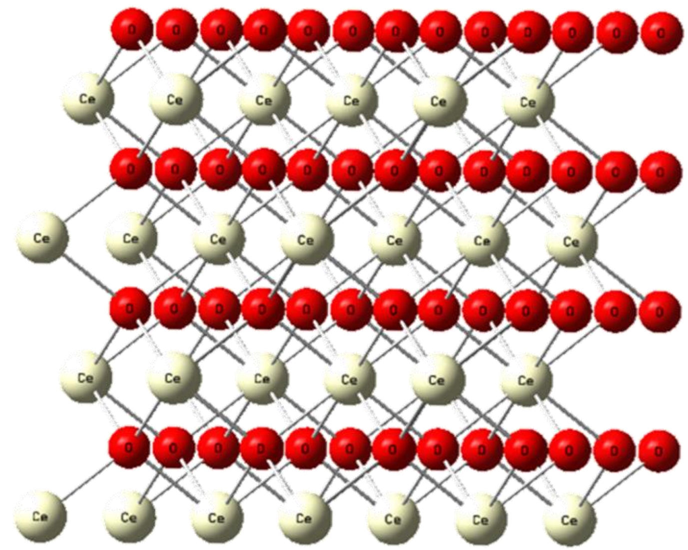

1. Water model
2. Hydroxide Model
3. Oxide surface
4. Absorption of radio nuclides onto the oxide surface.

Ongoing Work

Lancaster University

- Hydroxide Systems AIMD
  - Total simulation time of 100 ps
  - One final set of calculations to run to reach 100 ps
- Water Systems AIMD
  - Currently only 20 ps simulation time.
  - Repetition to 100 ps simulation time.
- CeO_2 Oxide Surface DFT + U
  - Optimisation of surface structure
  - Introduction of hydration models to surface

Any Questions?

- Theme 3 Annual Meeting
- 15th November 2016
- Olivia Lynes
- o.lynes@lancaster.ac.uk

Principles and effects of dynamic shear in micro and ultrafiltration of chalk suspensions

Keith Schou
Loughborough University

Ultra- & micro- filtration

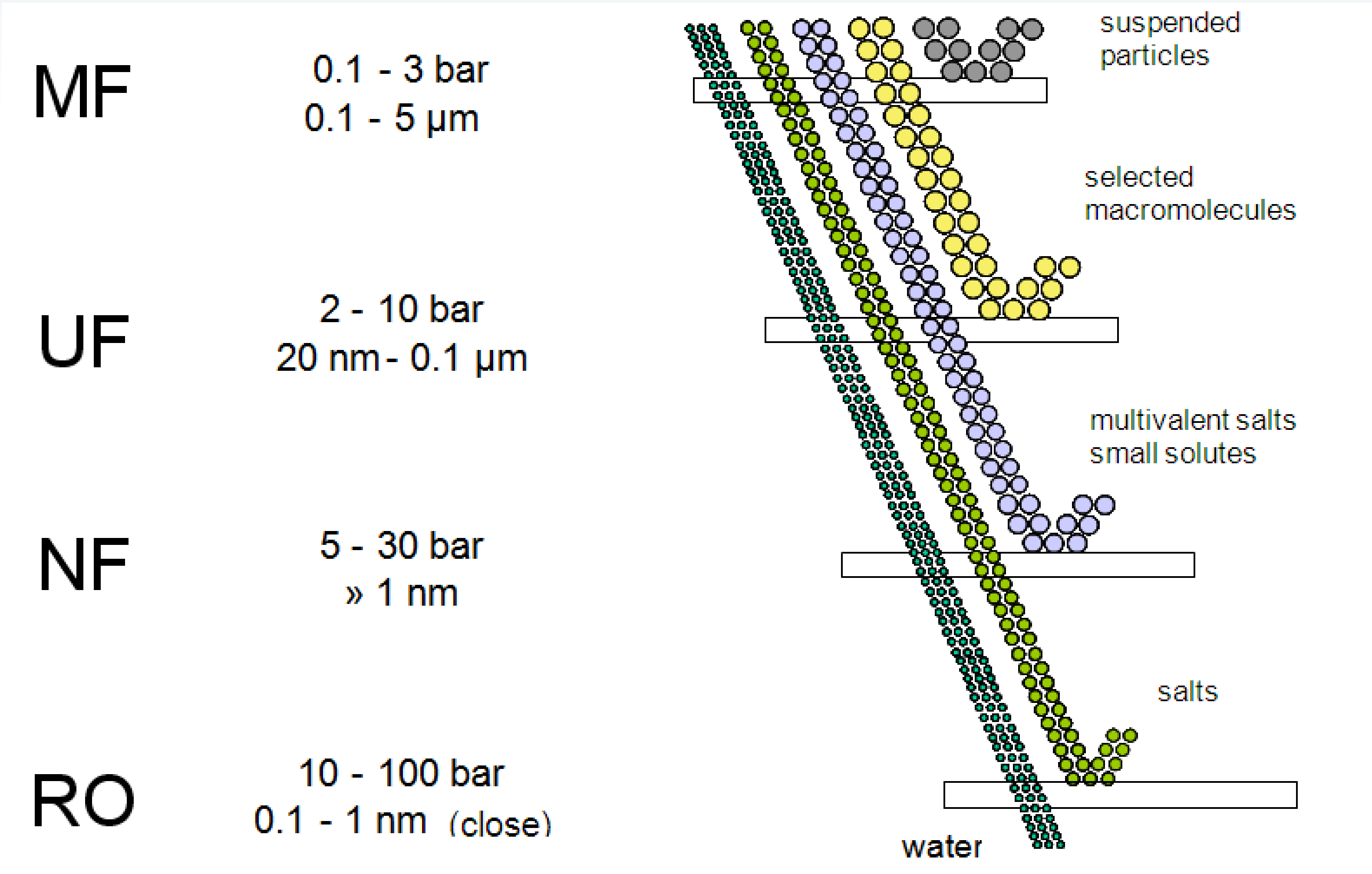

(Emis, 2015), retrieved from
http://emis.vito.be/sites/emis.vito.be/files/data_sheets/migrated/Microfiltration.png
accessed Apr/2015

Filter cake

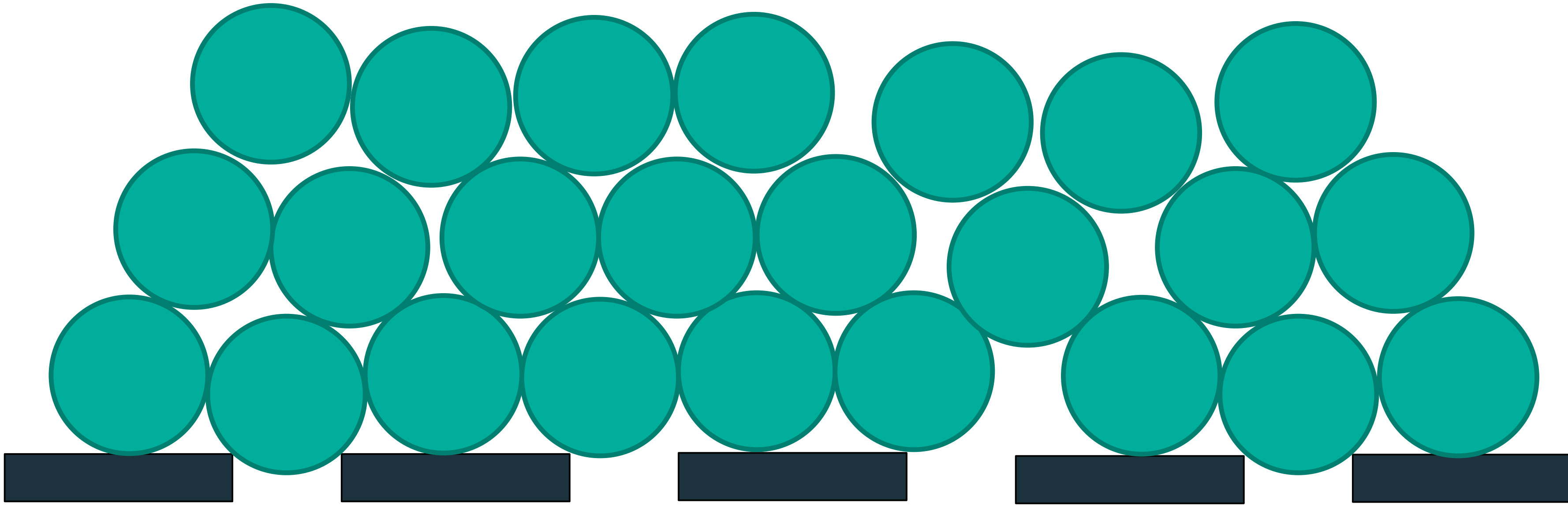

Where is this used

EARP

Enhanced Actinide
Removal Plant

Ferric floc
CMS

What is dynamic shear?

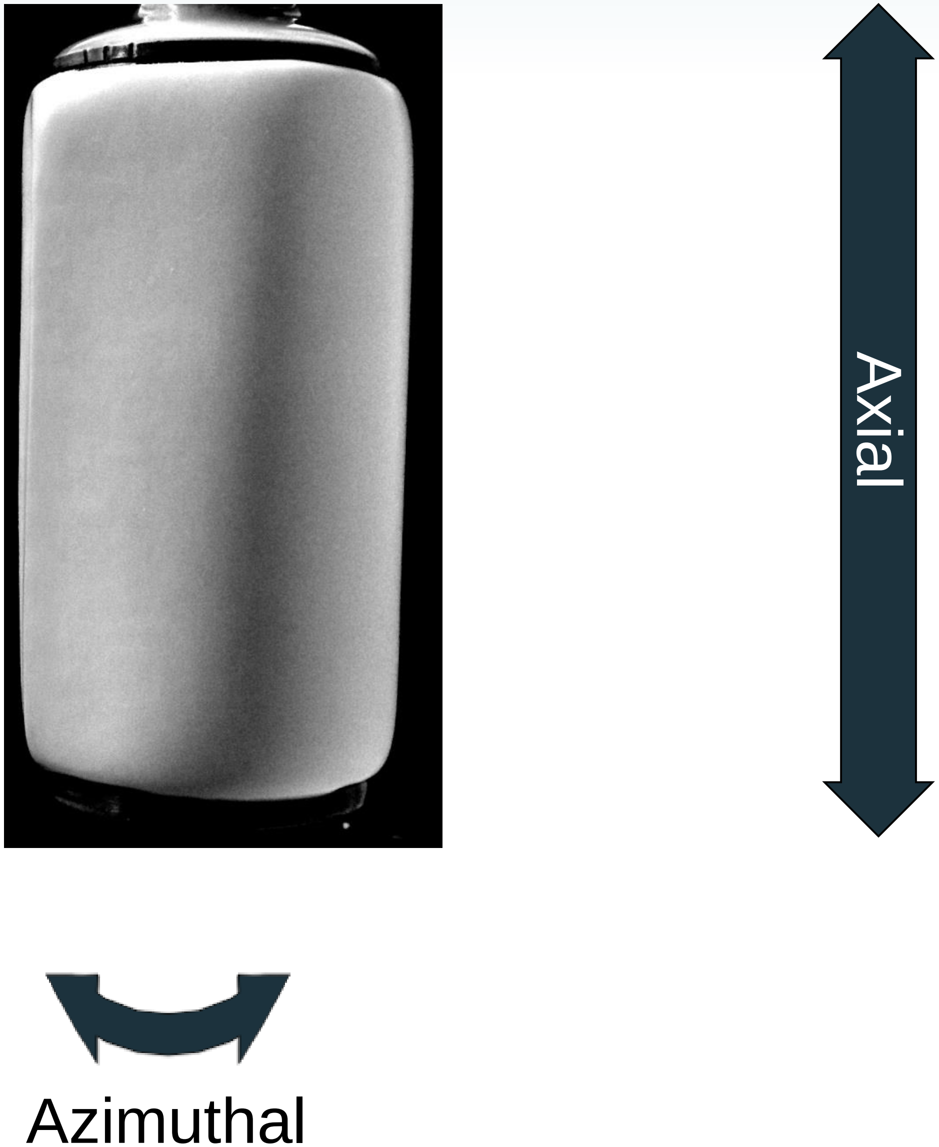

Dynamic shear systems

Commercial forms

- Vsep, New Logic
- SpinTek
- DYNO, Bokela
- OPTIFILTER, Metso paper
- FMX, BKT
- SSDF, Novoflow
- Westfilia Separator

In development

- Helical membranes
- Magnetically induced membrane vibrations
- Linear with turbulence promotors

Enhanced shear systems

Shear rate, γ (s^{-1})	Oscillation type	Flux Enhancement (E)	Reference	System
350	Axial	9.1	(Gomaa, Rao & Taweel 2011)	Linear with TP
2540	Axial	2.7	(Low et al. 2005)	Linear
4600	Axial	2.7	(Li et al. 2013)	Linear
18800	Axial	7.6	(Krantz et al. 1997)	Linear
33600	Azimuthal	2.1	(Kennedy et al. 1974)	VSep
38300	Azimuthal	4.1	(Low et al. 2004)	VSep
39000	Azimuthal	17.1	(Akoum et al. 2002)	VSep

Table 1 The enhancement factor as a function of average shear rate (Zamani et al. 2015)

Key research questions

- Does the application of the shear effect this enhancement?
- Does the filter used effect this enhancement?
- What are the underlying principles at work in this enhancement?
- Can these be characterised and modelled?
- Does the localised shear damage the suspension, creating a more difficult to filter suspension?
- How can this be applied in EARP

Experimental system

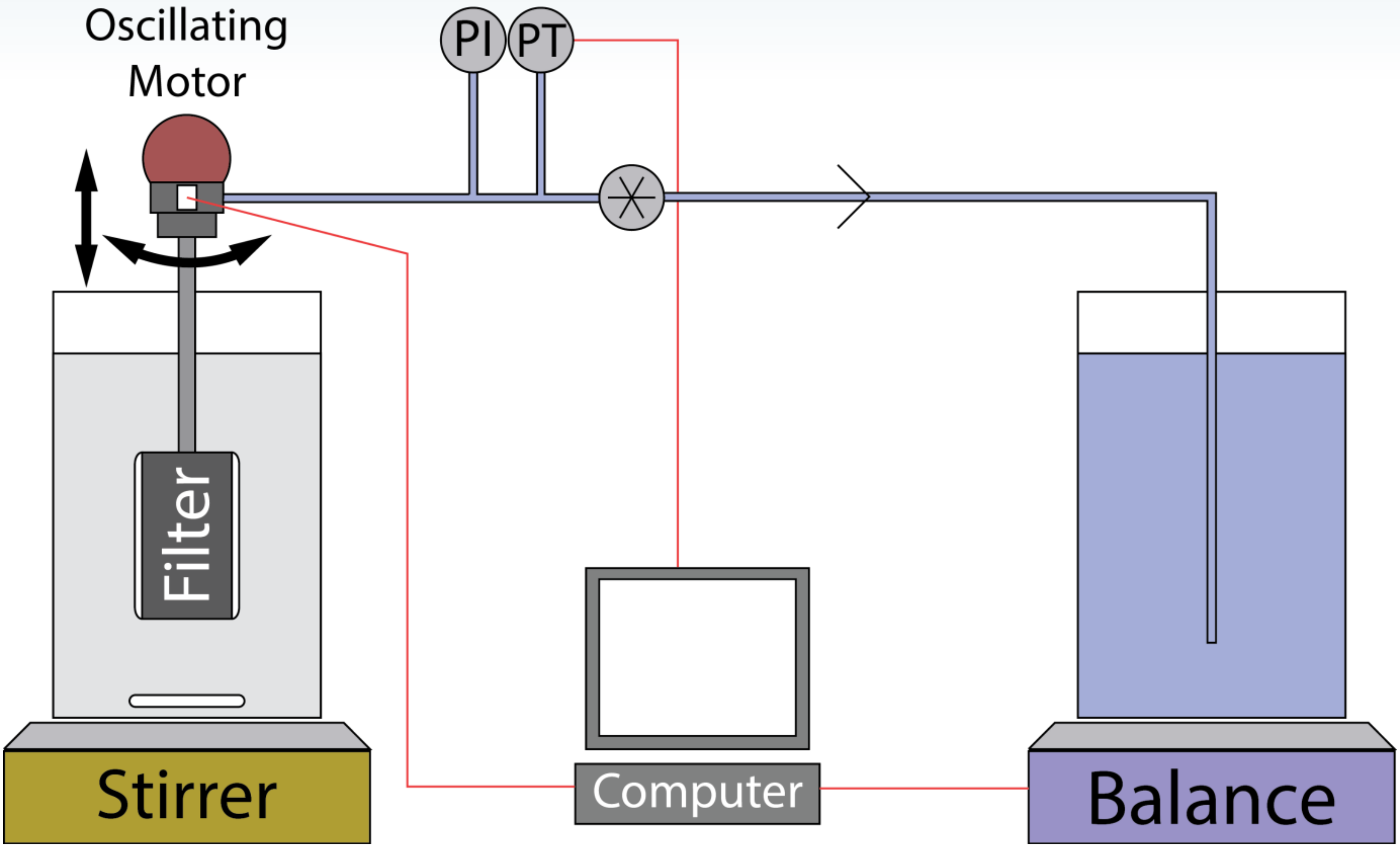

Filter / cake

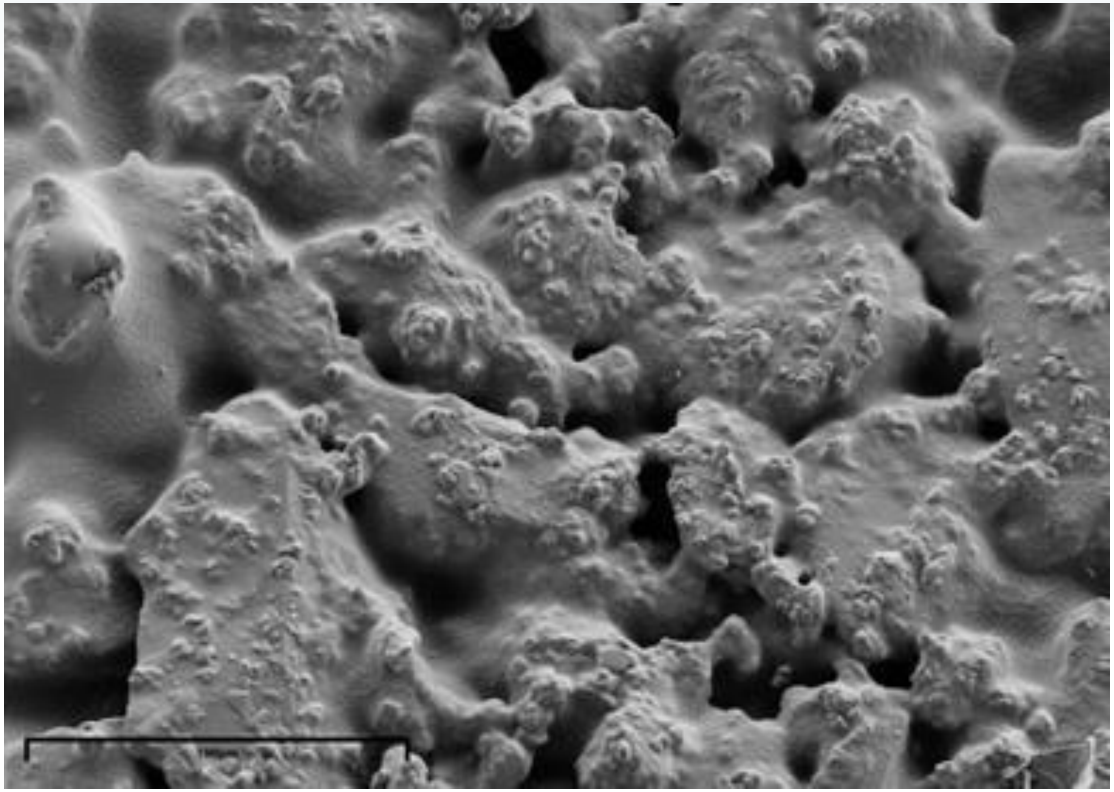

Suspension PSD

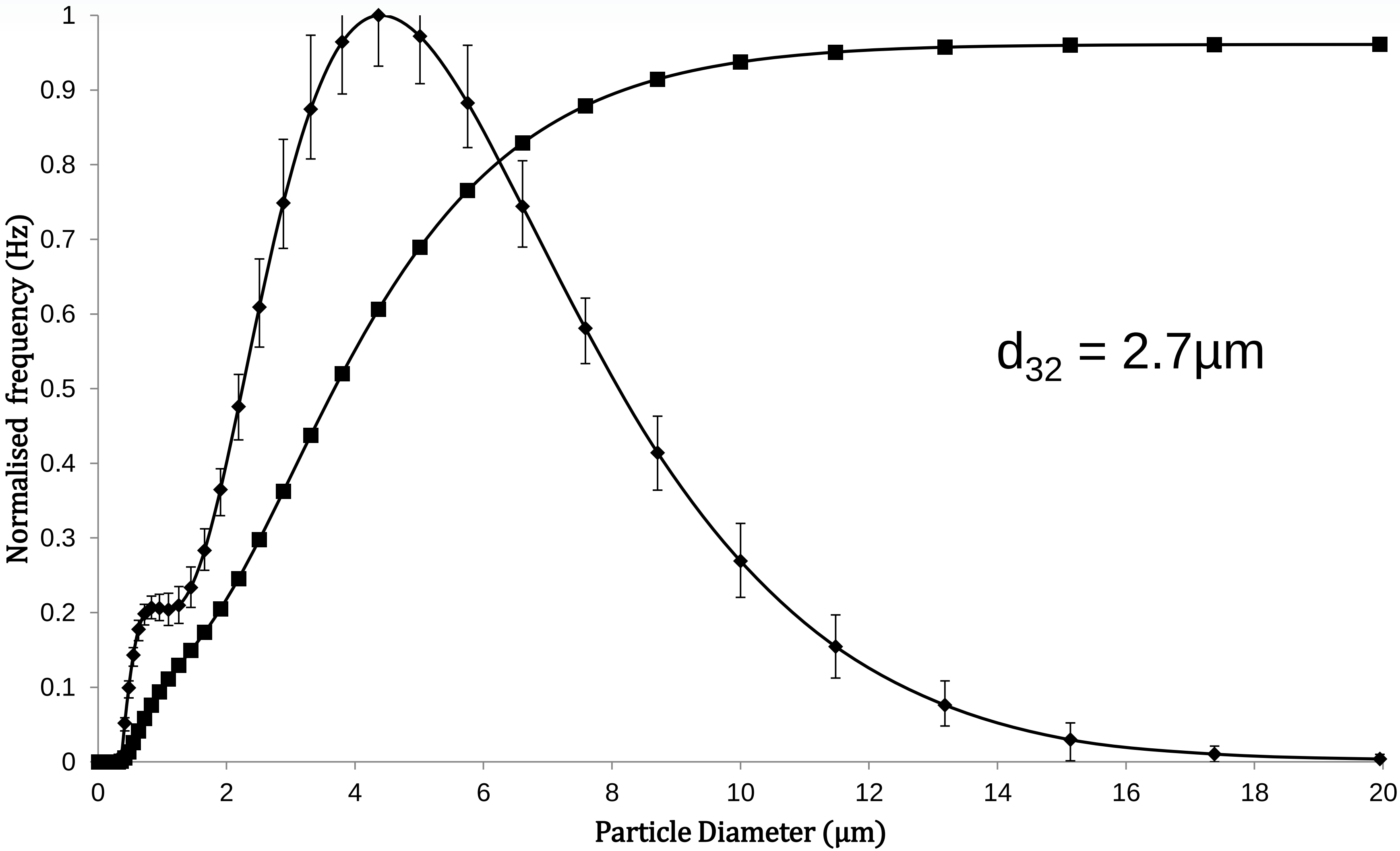

Cake Rheology

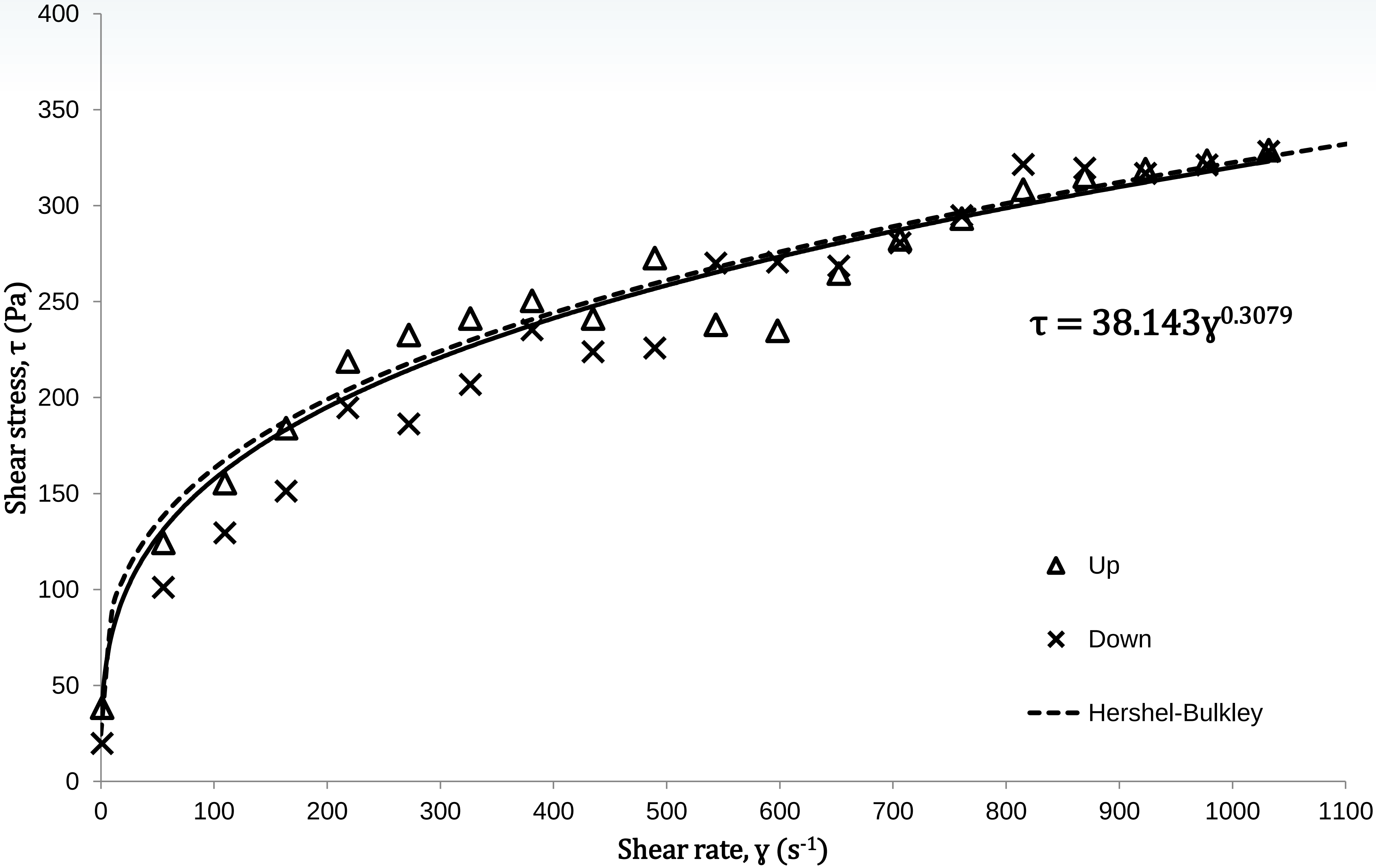

Cake Depth

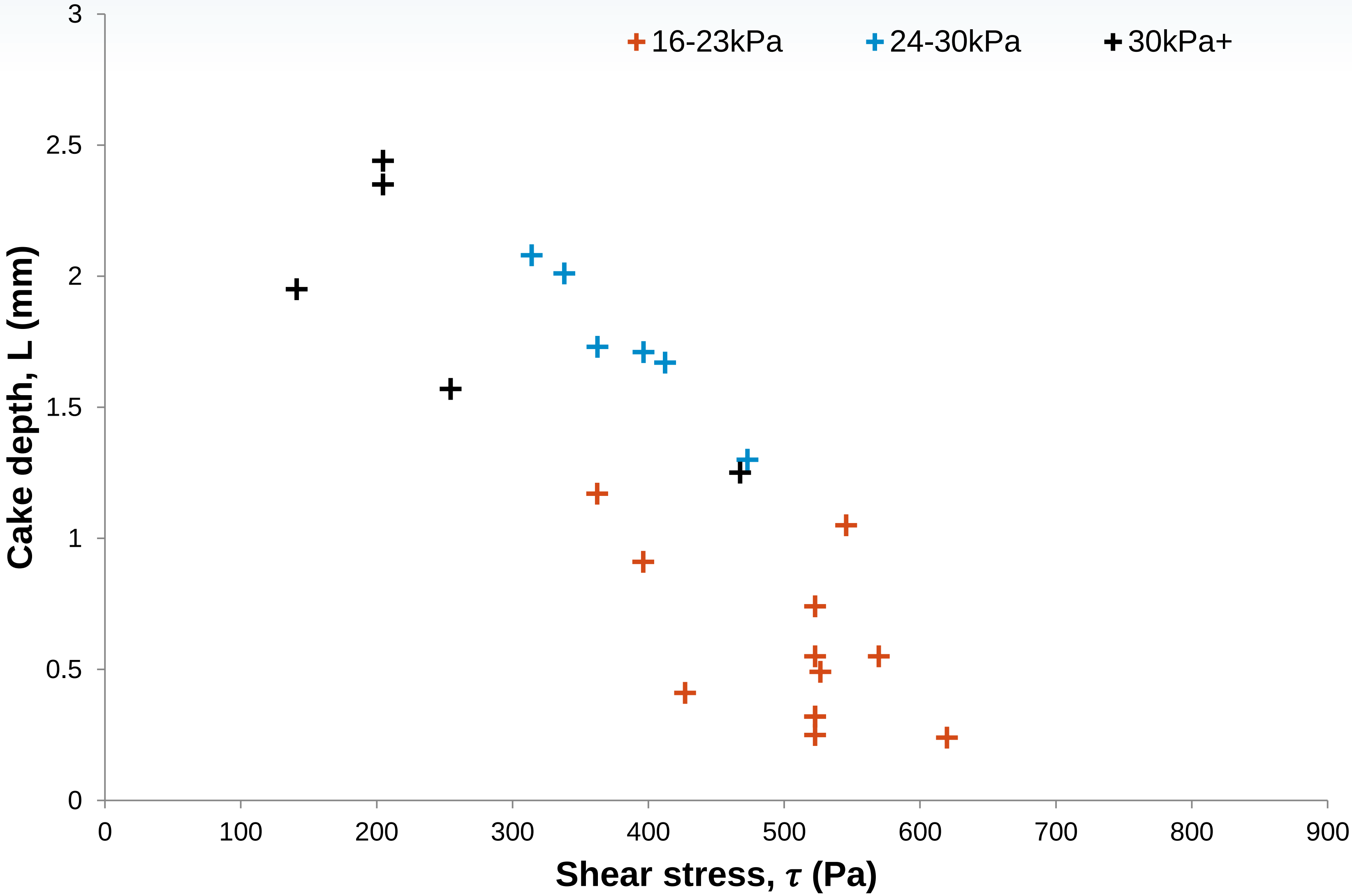
16-23kPa
24-30kPa
30kPa+
Cake depth, L (mm)
Shear stress, τ (Pa)
0
0.5
1
1.5
2
2.5
3
0
100
200
300
400
500
600
700
800
900

Resistance

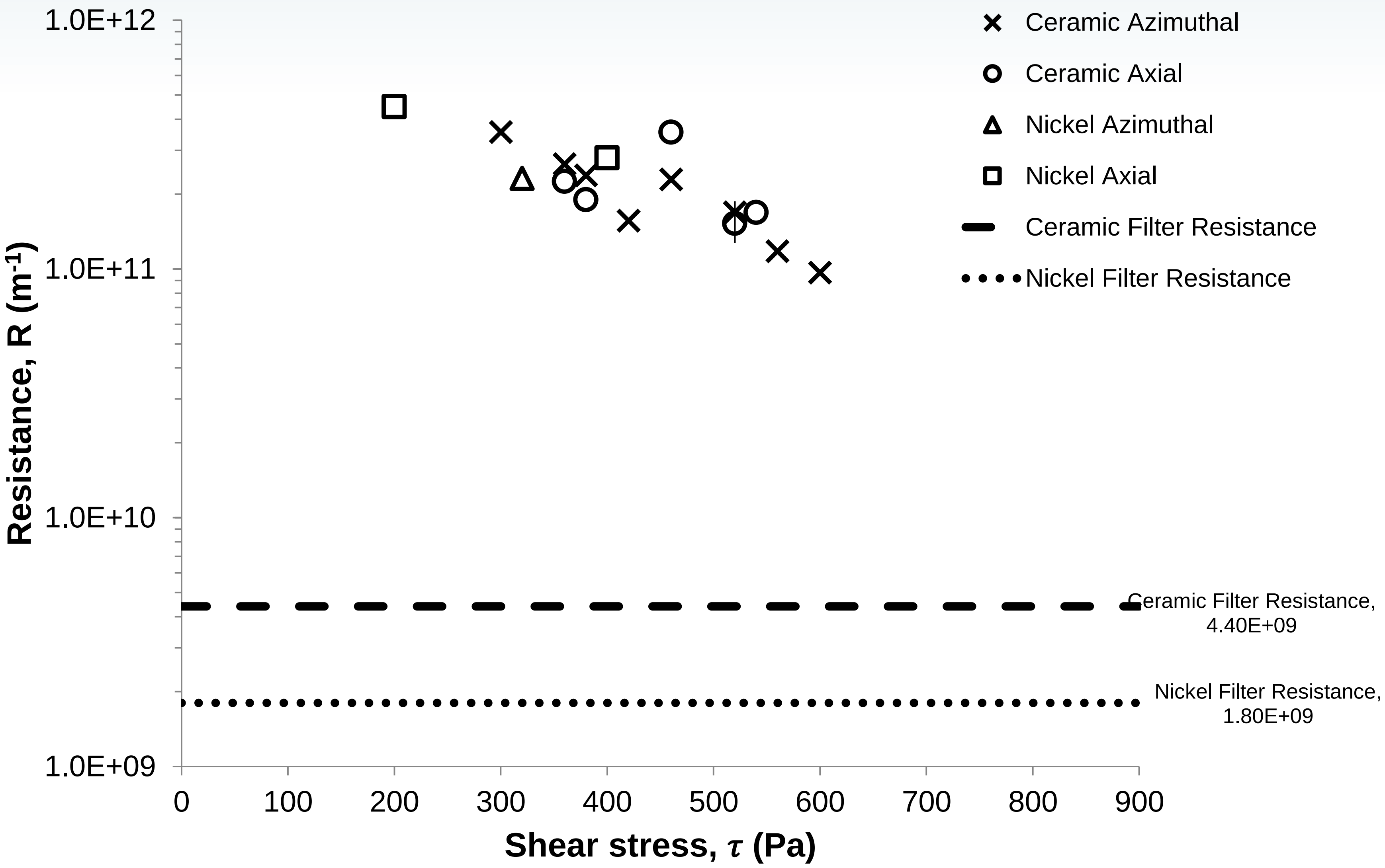

1.0E+12
1.0E+11
1.0E+10
1.0E+09
Resistance, R (m^{-1})
0
100
200
300
400
500
600
700
800
900
Shear stress, τ (Pa)
Ceramic Azimuthal
Ceramic Axial
Nickel Azimuthal
Nickel Axial
Ceramic Filter Resistance
Nickel Filter Resistance
Ceramic Filter Resistance, 4.40E+09
Nickel Filter Resistance, 1.80E+09

Nomenclature

Variable	Symbol	Units
Area	A	m^2
Amplitude	a	m
Cake concentration	C	
Particle diameter – Sauter mean	d_{32}	m
Frequency	f	s^{-1}
Flux	J	$m^3.m^{-2}.s^{-1}$
Cake permeability	k	m^2
Cake thickness	L	m
Trans membrane pressure	ΔP	Pa
Volumetric flowrate	Q	$m^3.s^{-1}$
Resistance	R	m^{-1}
Pore diameter	rp	m
Shear stress	τ	Pa
Viscosity (permeate)	μ_p	Pa.s
Shear Rate	γ	s^{-1}

Maths of the system

$$\gamma_{Max} = 2\pi f a \sqrt{\frac{2\pi f}{2\eta}}\sqrt{2}$$

- Wave equation

$$\tau = K\gamma^{m}$$

- Power law (from rheology)

$$J = Constant_1 . \gamma^{Constant_2}$$

- From literature

(Jaffrin et al. 2004; Akoum et al. 2002; Petala & Zouboulis 2006; S. P. Beier et al. 2006; Genkin et al. 2006; Gomaa, Rao & Al-Taweel 2011; Postlethwaite et al. 2004; Akoum et al. 2005)

$$J = K_1 d_{32}\tau + K_0$$

- Friction equation

$$R = \frac{A}{\mu_p}\frac{\Delta P}{Q} \qquad k = \frac{L}{R} \qquad Q = \frac{k\Delta P A}{L\mu_p}$$

- Darcy's equation (different forms)

Maths of the system

$$J = K_1 d_{32}\tau = \frac{k\Delta P}{L\mu_p}$$

Happel and Brenner model

$$k = \frac{\left(2 - 3C^{\frac{1}{3}} + 3C^{\frac{5}{3}} - 2C^2\right)}{\left(3 + 2C^{\frac{5}{3}}\right)} \frac{{d_{32}}^2}{12C}$$

$$K_1 = \frac{k\Delta P}{L\mu_p d_{32}\tau}$$

$$L = \frac{{d_{32}}^2(1 - C)\Delta P}{90\tau C^2\sqrt{{d_{32}}^2 - 4rp^2}}$$

Maths of the system

$$J = \frac{15\tau C\left(2 - 3C^{\frac{1}{3}} + 3C^{\frac{5}{3}} - 2C^{2}\right)\sqrt{{d_{32}}^{2} - 2\left(\frac{\sqrt{9{d_{32}}^{4} + 16{d_{32}}^{2}}}{4} - d_{32}\right)^{2}}}{2\left(3 + 2C^{\frac{5}{3}}\right)(1 - C)\mu_p}$$

Great!.... But it doesn’t work

Friction model

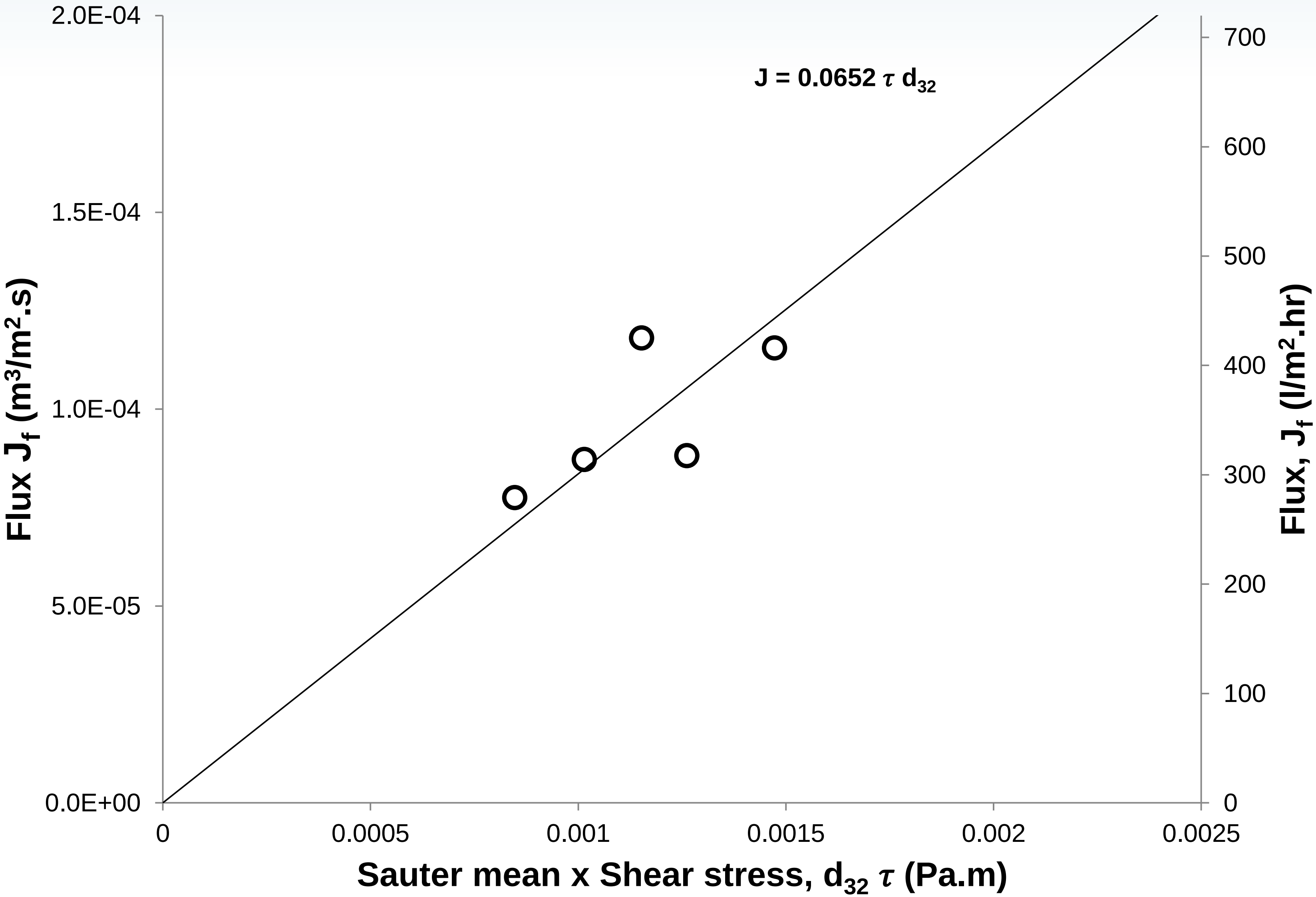

Shear vs flux

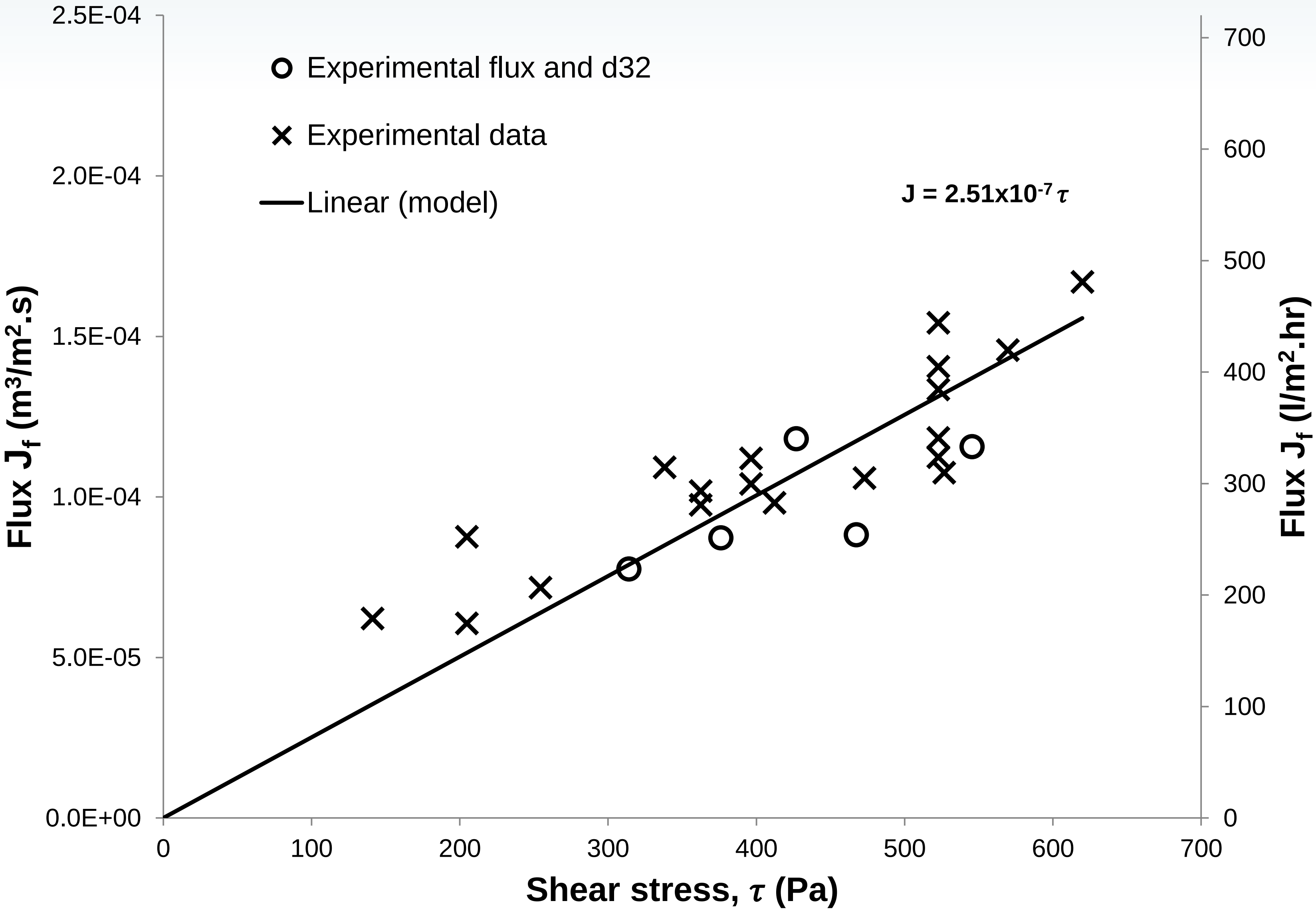

Striations

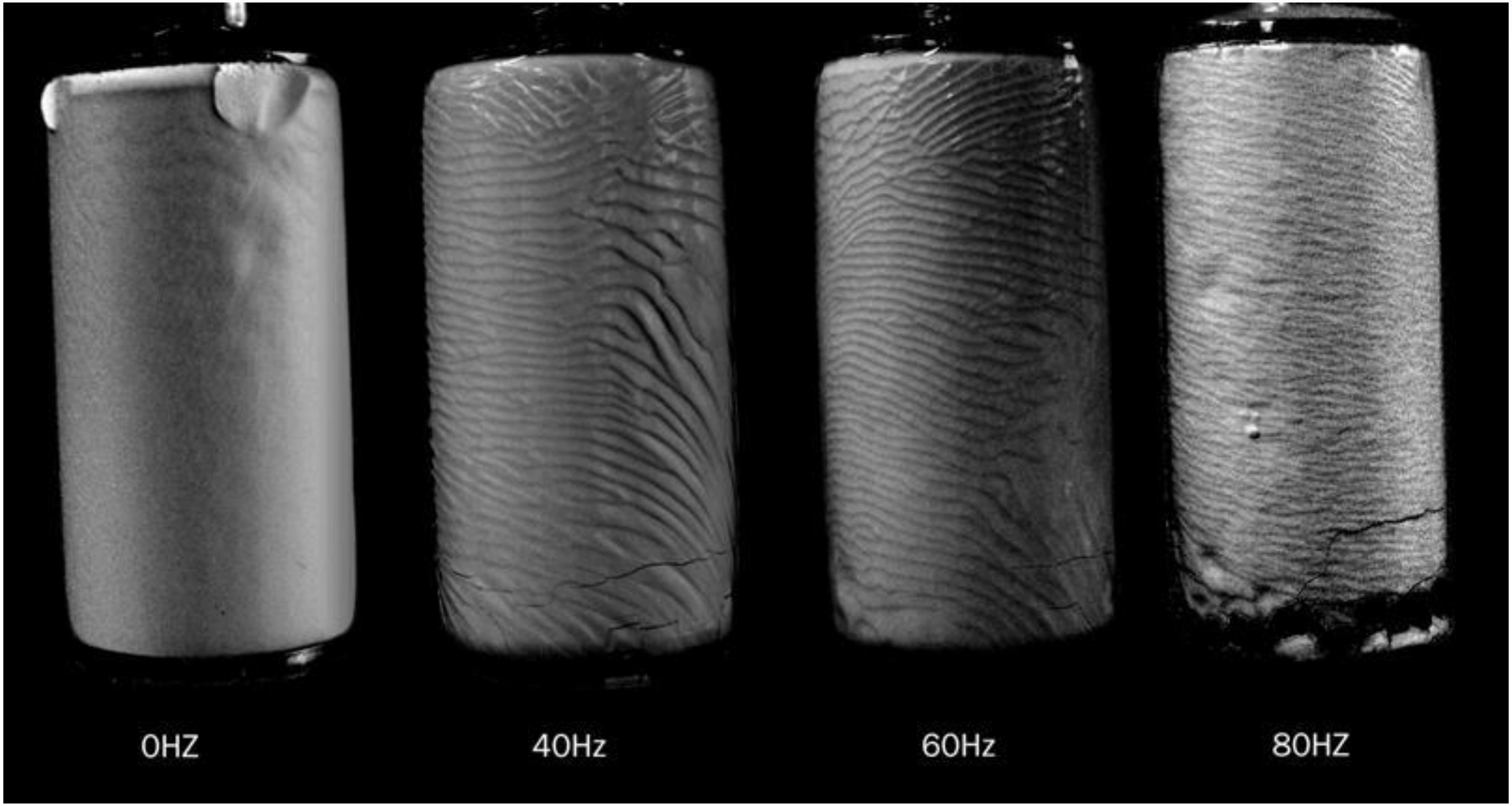

High Speed Film

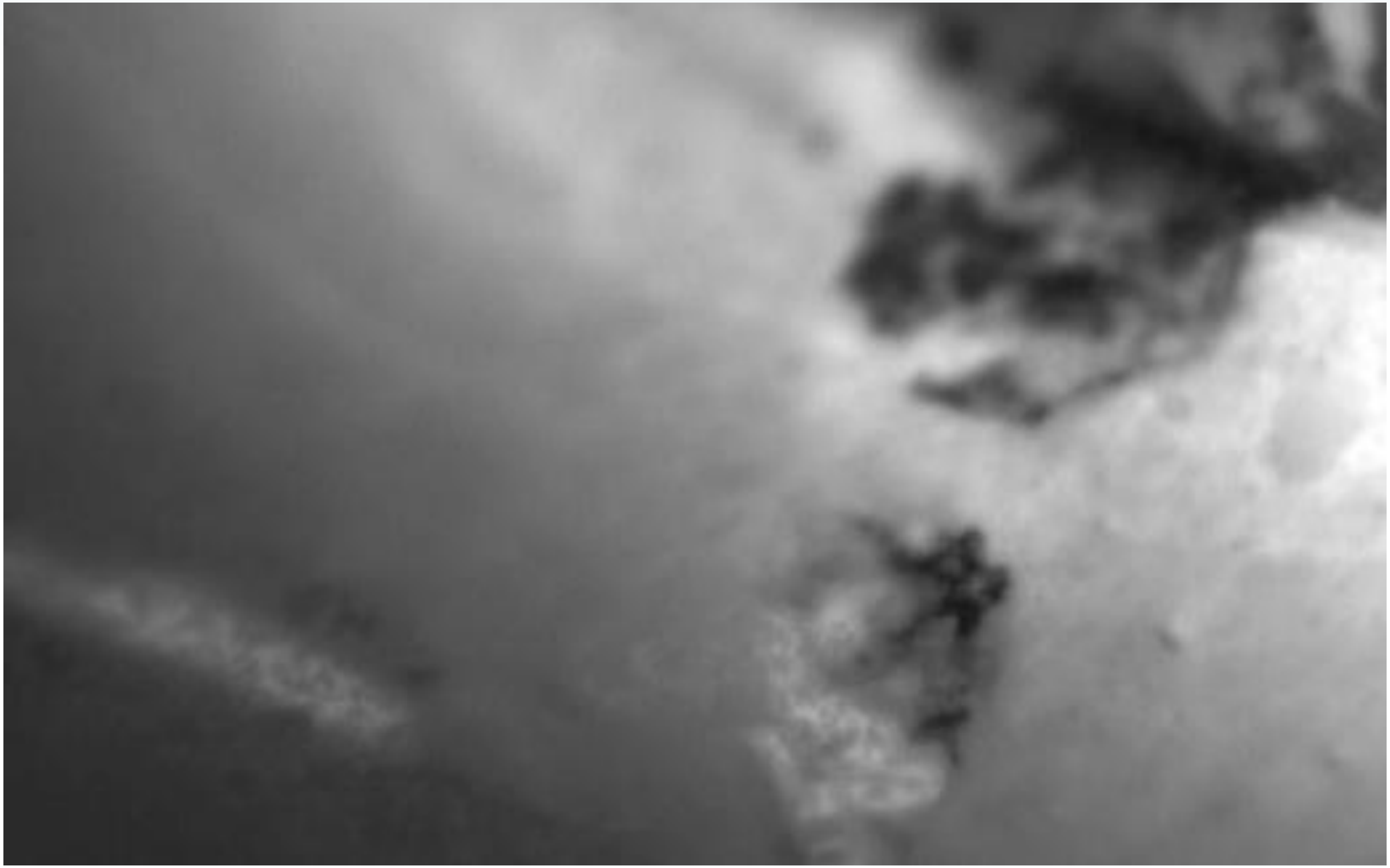

MgOH

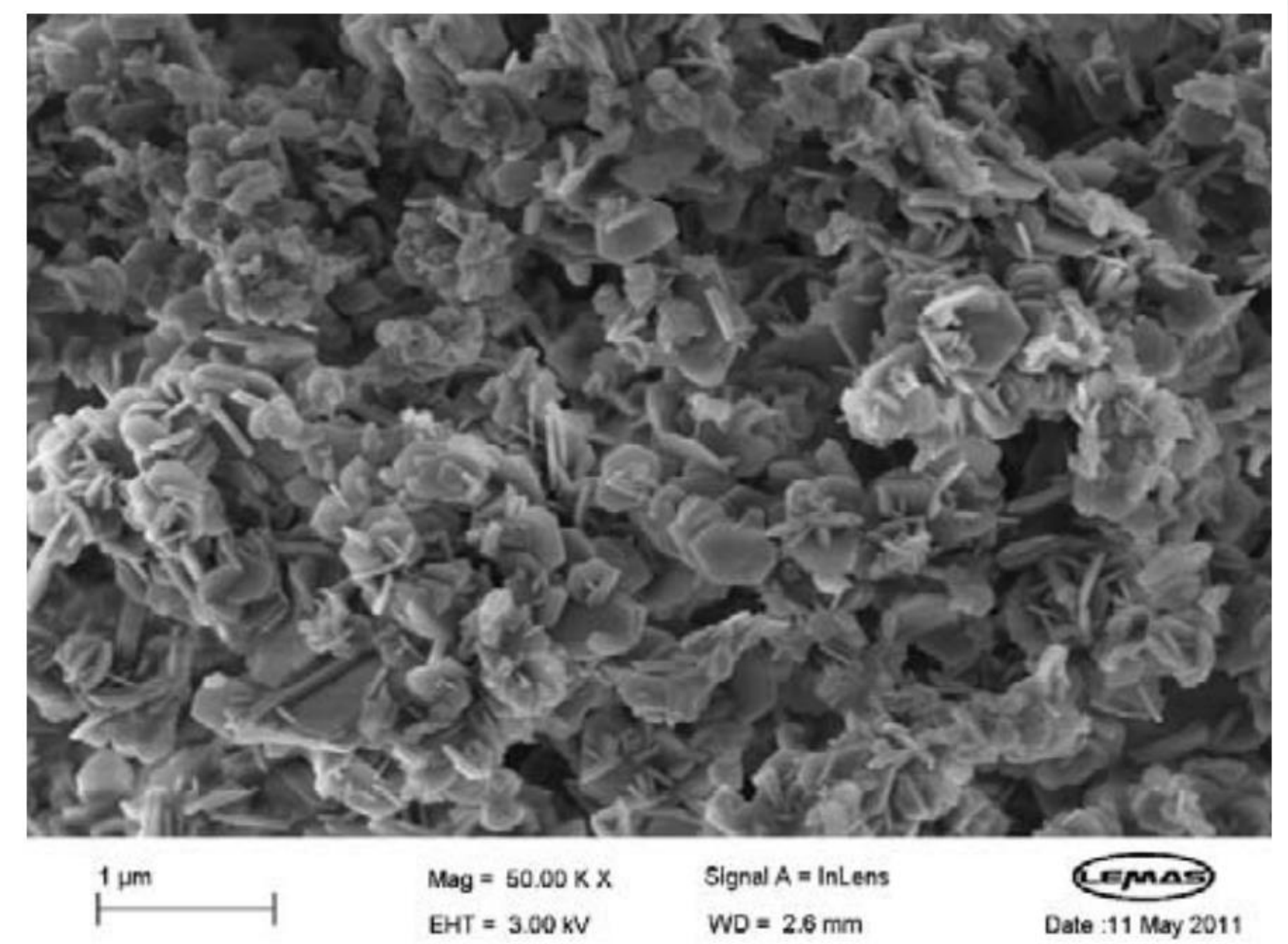

Image taken from Technology Development and Delivery Summary 2011 – Sellafield sites

Ferric floc

- Used in EARP

- Co-precipitates heavy metal ions

- Needs to be concentrated / dewatered

- Is a much ‘fluffier’ and ‘stickier’ substance than minerals (i.e. $CaCO_3$ and MgOH)

Future work

- Intend to investigate the following:
  - Numerical simulation (COMSOL) – to understand shear at the cake surface
  - Cake formation – fundamentals (further work required)
  - $Mg(OH)_2$
  - Ferric Floc
  - Design application

Conclusions

- Particle retention relies on the formation of a filter cake
- The resistance to filtration, and therefore the flux rate are dependent on the cake thickness
- There is a very strong correlation between cake thickness and shear stress
- The friction model is described by a large number of authors, and when applied, along with other derivations a predictive model can be constructed.
- The current predictive model of L is not accurate.
- The formation of the filter cake is independent on the type of shear (azimuthal or axial)
- The type of filter used has negligible effect on the overall resistance, provided a cake is formed, as the resistance is dependent on that cake.

Questions

?

Permeability

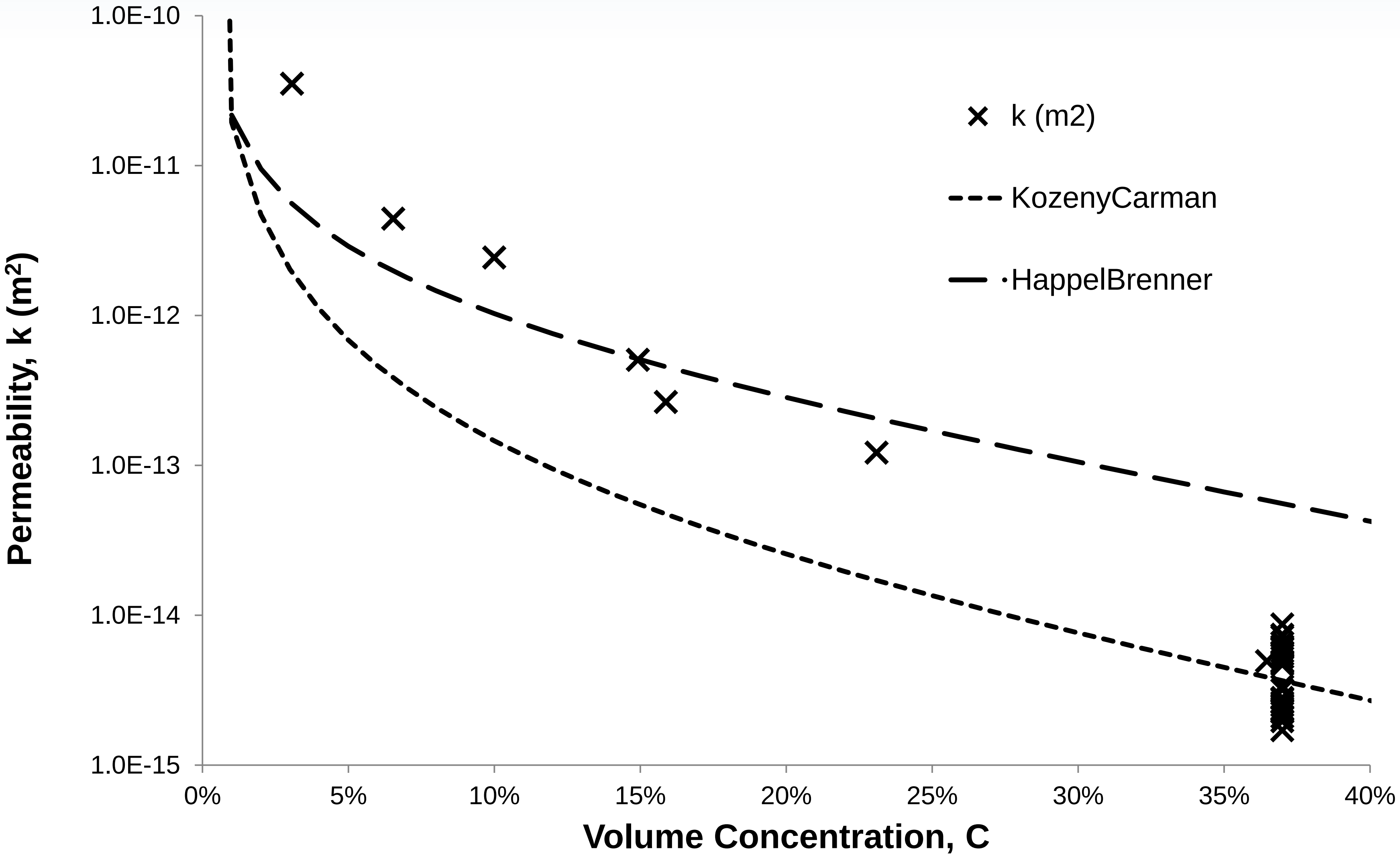

Sauter mean of cake

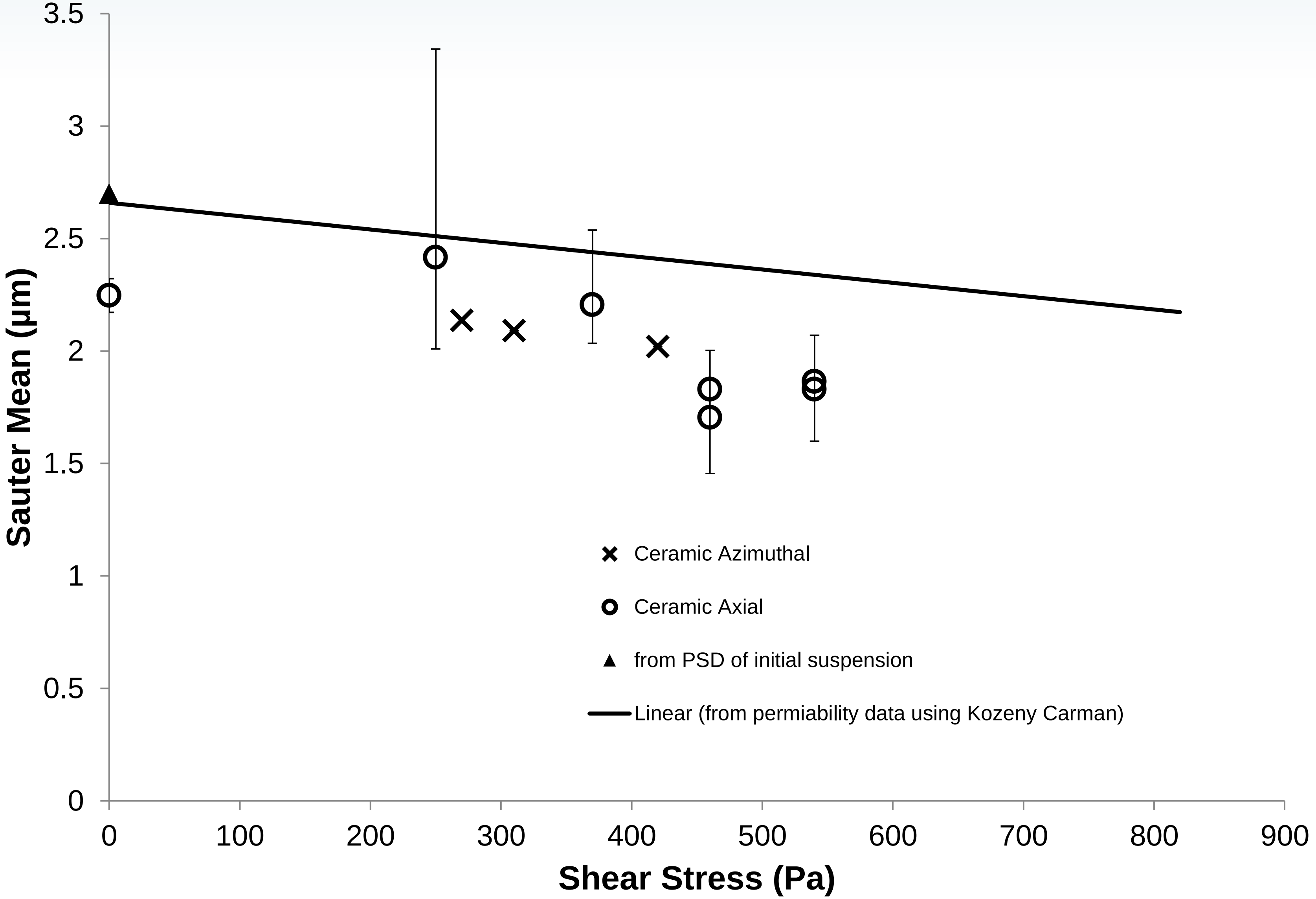

The evolution of bubble populations in Magnox legacy waste

Michael Johnson, Timothy Hunter, David Harbottle, Jeff Peakall,
Michael Fairweather and Simon Biggs

University of Leeds
School of Chemical and Process Engineering

November 2016

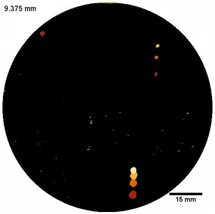

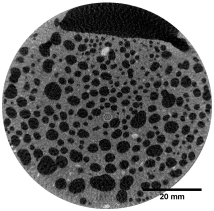

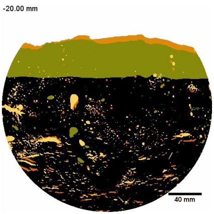

Gas retention in legacy waste

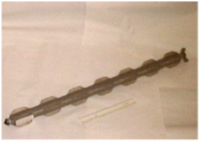

A - Magnox Fuel Can

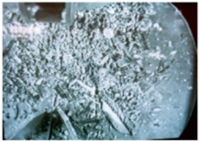

B - Magnox - *Partially Corroded Swarf and Magnesium Hydroxide Sludge*

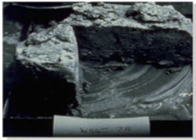

C - Magnox Sludge - *Active Magnesium Hydroxide Sludge Sample*

Hastings *et al.* 2007

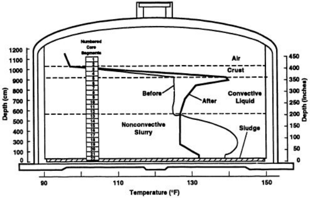

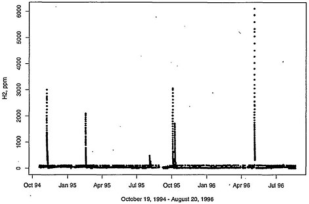

Allemann 1992

$$\mathrm{Mg} + 2\,\mathrm{H_2O} \longrightarrow \mathrm{Mg(OH)_2} + \mathrm{H_2} \quad (1)$$

- Magnox cladding corrodes and consolidates into dense beds of CMS
- Hanford engineers have observed periodic upward transfers of decay heat coinciding with spikes in $\mathrm{H_2}$ concentration in the ullage, considered to be *rollover events*

Test material characterisation

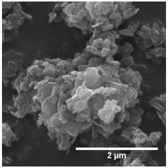

SEM

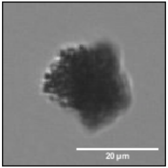

Sysmex

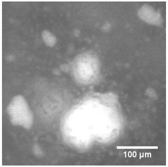

PVM
Johnson *et al.* 2016

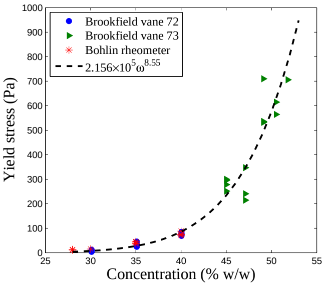

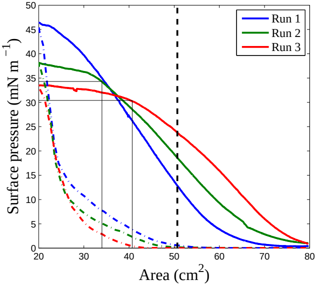

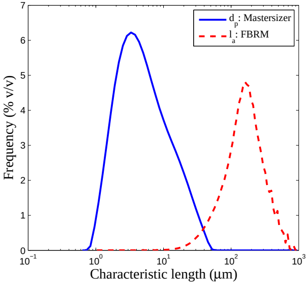

Gas retention tests

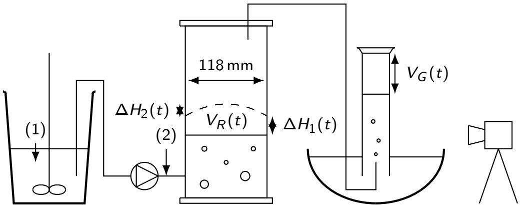

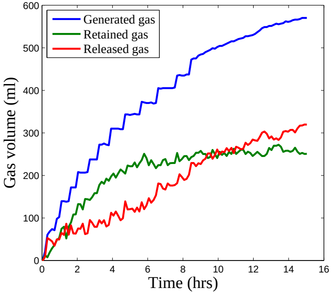

$$\mathrm{H_2O_2} \longrightarrow \mathrm{H_2O} + \tfrac{1}{2}\,\mathrm{O_2} \tag{2}$$

$$V_R(t) = \pi R^2 \Delta H_1(t) + \frac{1}{3}\pi \Delta H_2(t)^2 \left(3R - \Delta H_2(t)\right) \tag{3}$$

$$V_G(t) = V_R(t) + V_E(t) \tag{4}$$

Feasibility of rollover events

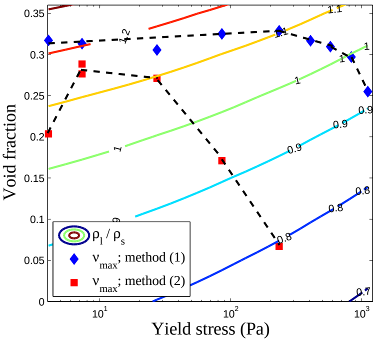

- Void fractions upward of 30 % are observed in sediments of $\tau < 600$ Pa
- Sediments of $\tau < 800$ Pa can experience sufficient *bed swell* to potentially induce *rollover*
- Continuous injection of $\mathrm{H_2O_2}$ into the feedline significantly reduces the capacity for bed expansion, especially in weak ($\tau < 30$ Pa) and medium strength ($80 < \tau < 240$ Pa) sediments

X-ray CT: imaging methodology

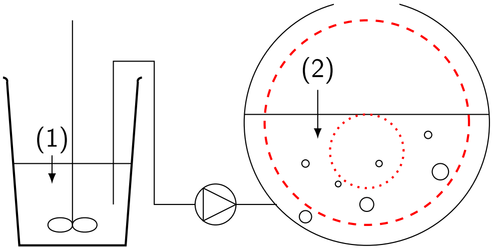

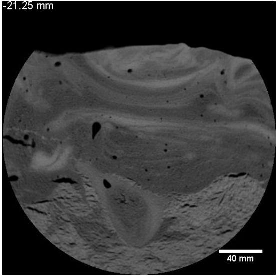

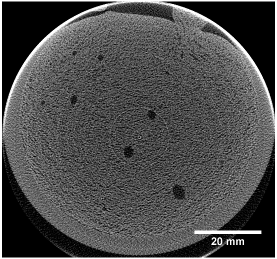

	GE Brivo		Siemens Inveon
	Large FOV	Small FOV	
X-ray voltage (kV_p)	120	120	80
X-ray tube current (mA)	40	79	0.5
FOV diameter (mm)	250	96	81.8
Pixel resolution (μm)	488	250	53.25
Slice separation (μm)	1250	625	53.25
Number of axial slices	112	32	1024
Axial FOV depth (mm)	138.8	19.4	54.5
Total FOV volume (mm^3)	6.81×10^6	1.40×10^5	2.86×10^5

Evolution in bubble size and number

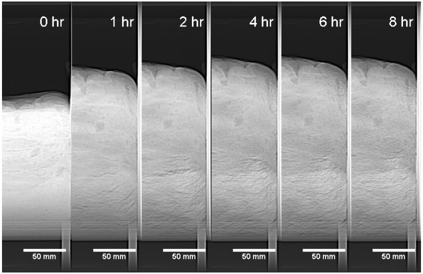

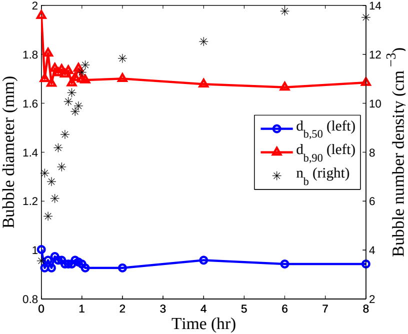

- Bed expansion occurs within the first 4 h
- The median and d_{90} bubble sizes (mature bubbles only) reach a steady state within the first hour
- The increase in voidage is mirrored by the increase in number of mature (millimetre scale) bubbles

Impact of yield stress on bubble size and shape

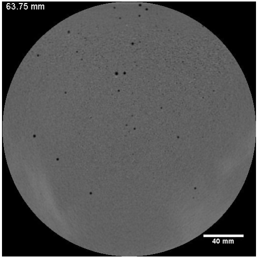

7 Pa

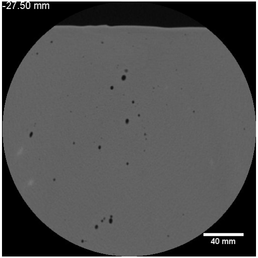

86 Pa

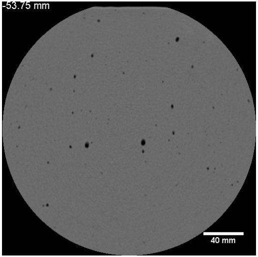

234 Pa

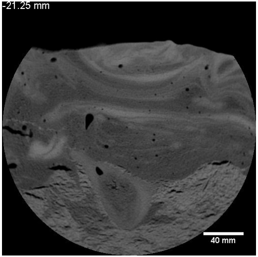

1112 Pa

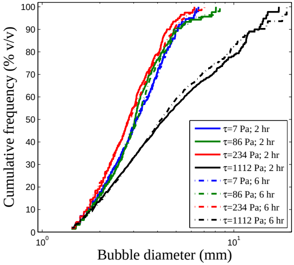

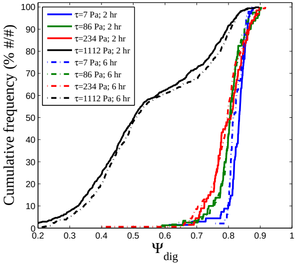

Bubble motion and residence times

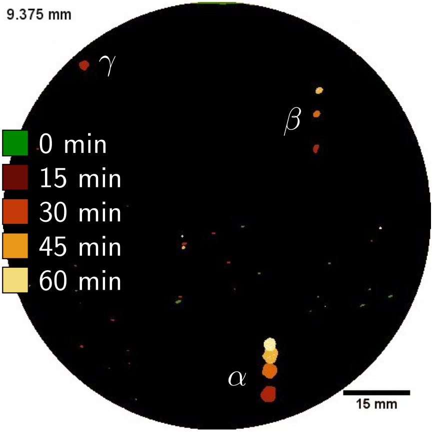

7 Pa

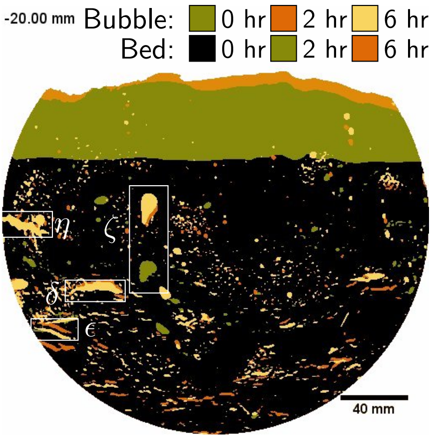

1112 Pa

Non-homogeneous gas generation

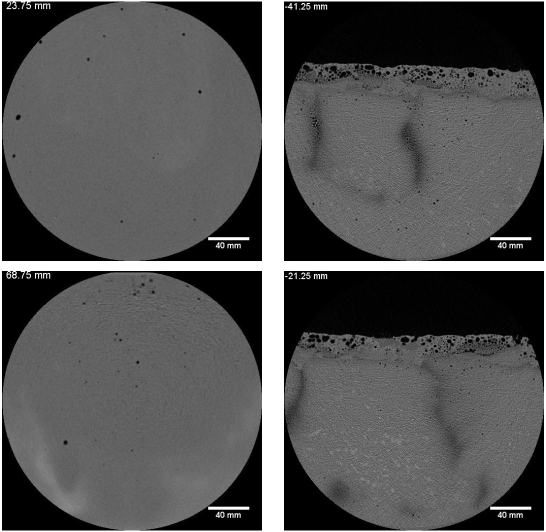

Method (1) Method (2)

- Homogenous distribution of peroxide results in greater bulk bed expnansion (or a reduced rate of gas release)
- Less homogeneous distribution of volatiles resulted in (1) a high porosity foam layer at the surface and (2) dark regions of low radiodensity

Comparison of test materials

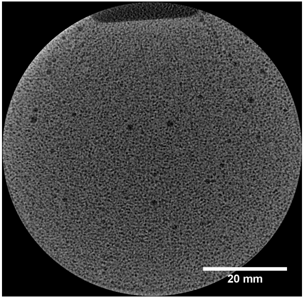

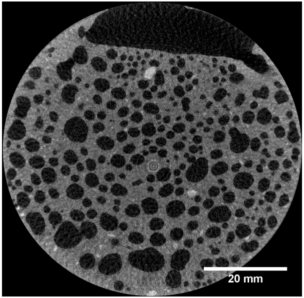

- Higher resolution ($d_{vox} = 53.25\,\mu m$) CT images captured at the Centre for Advanced Imaging, University of Queensland
- CMgS exhibits a vastly coarser bubble population after 6 h *in situ* gas generation than the commercial $\mathrm{Mg(OH)_2}$ ($\tau \approx 30\,\mathrm{Pa}$ for both samples)

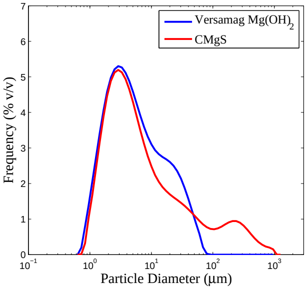

Pore scale bubble growth

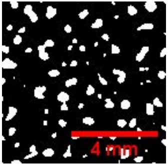

27 Pa

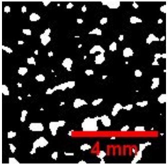

234 Pa

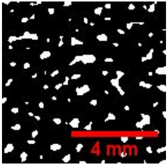

1111 Pa

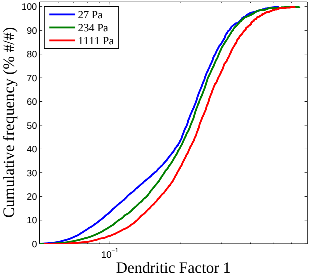

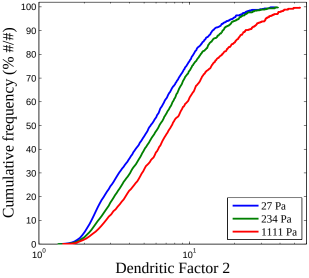

$$DF1 = \frac{\sigma_{d_i}}{d_b} \tag{5}$$

$$DF2 = \frac{V_{Bound}}{V_b} \tag{6}$$

$$\frac{\Delta P_{CI}}{\Delta P_{CE}} = \frac{\frac{\gamma}{r_{th}} cos(\theta)}{\frac{4}{3}\tau \left(1 + ln \left| \frac{G}{\tau} \right| \right)} \propto \frac{\gamma cos(\theta)}{\tau r_{th}} \tag{7}$$

Forthcoming work

1. Couple the pore scale bubble growth results with micro-CT characterisation of the two-phase pore structure
2. Investigate the mechanics and flow behaviour of gassy soft sediments
3. Investigate the growth kinetics and buoyant motion of bubbles from a single submerged orifice

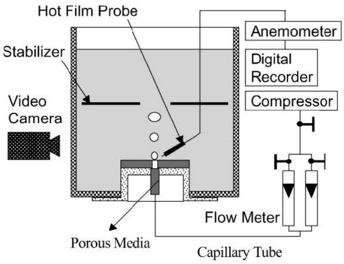

from Zhang and Shoji 2001

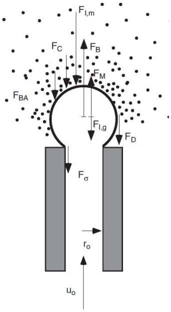

from Yang *et al.* 2007

Conclusions

1. Sediments of $\tau < 800\,\text{Pa}$ can experience sufficient *bed swell* to potentially induce *rollover events*
2. Continuous injection of $\mathrm{H_2O_2}$ into the feedline resulted in localised pockets of gas generation resulting in low density regions, rich in microbubbles, which appear to facilitate enhanced gas release
3. Sediments $> 1\,\text{kPa}$ exhibit bubble growth by induction of lateral fractures which appear to enable gas transport to the bed periphery
4. Sediments of $7 < \tau < 234\,\text{Pa}$ retain virtually identical size distributions of mature bubbles, implying a release mechanism unrelated to bubble buoyancy
5. Pore scale bubbles appear to become more dendric with increased bed strength
6. Corroded magnesium metal sediments appear to support much coarse bubble size distributions than commercial $\mathrm{Mg(OH)_2}$ sediments

Thank you for listening

Supervisors and collaborators

Tim
Hunter

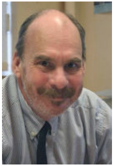

Mike
Fairweather

Dave
Harbottle

Jeff
Peakall

Simon
Biggs

...with thanks also to Geoff Randall and Martyn Barnes of Sellafield Ltd.

and for funding and support from

Sellafield Ltd EPSRC NDA Nuclear Decommissioning Authority UNIVERSITY OF LEEDS

School of Electronic and Electrical Engineering
FACULTY OF ENGINEERING

UNIVERSITY OF LEEDS

Novel Characterisation of Flocculated Dispersions using Acoustic Backscatter Systems

Alastair Tonge

Supervisors: Dr Tim Hunter, Prof Steven Freear & Prof. Jeff Peakall

Acknowledgements

UNIVERSITY OF LEEDS

- Sellafield and the NDA
- Martyn Barnes & Geoff Randall
- Hugh Rice and Jaiyana Bux
- Dr Tim Hunter, Prof. Jeff Peakall and Prof. Steven Freear

Motivation - Aims of acoustic characterisation

UNIVERSITY OF LEEDS

First Generation Magnox Storage Pond - Sellafield

Water Treatment Thickener

- **Analysis of settling front and concentration profiles in small-scale test settling suspensions.**
- **Modelling prediction and *In situ* monitoring of sludges to optimise of processing, transport and separation.**
- **Additional applications in water treatment & minerals thickeners**

Major advantage: Ability to observe changes in visually opaque suspensions

Motivation – Sellafield Pile Fuel Storage Pond

UNIVERSITY OF LEEDS

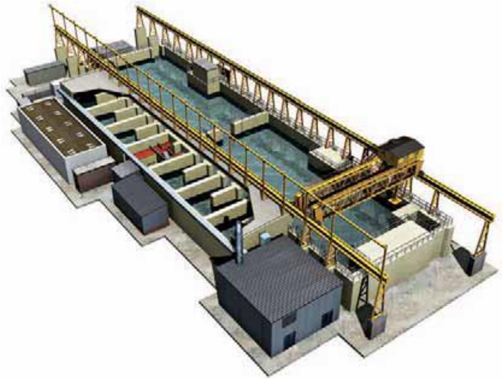

- Spent fuel from the first Windscale pile reactors has been stored in the PFSP for > 50 years.
- Corrosion of the waste material and additional organic mater has resulted in a significant build up of sludge.
- Sludge recovery is on-going as part of a decommissioning programme with settlement in a corral prior to removal for ultimate encapsulation.

Measurement principle

UNIVERSITY OF LEEDS

$$V_{\mathrm{rms}} = \frac{k_s k_t}{\psi r} C^{\frac{1}{2}} e^{-2r(\alpha_w + \alpha_s)}$$

k_s	particle species backscatter co-efficient
k_t	transducer constant
ψ	near field correction factor
r	distance from transducer face
$\boxed{C}$	$\boxed{\text{mass concentration}}$
α_w	attenuation of water
α_s	attenuation of suspended particles

P. D. Thorne and D. M. Hanes, “A review of acoustic measurement of small-scale sediment processes,” *Continental Shelf Research,* vol. 22, pp. 603-632, 2002.

Measurement principle

$$G = \ln(\psi r V_{\mathrm{rms}}) = \ln(k_{sh} k_t) + \frac{1}{2}\ln C - 2r(\alpha_w + \alpha_{sh})$$

k_{sh}	particle species backscatter co-efficient (under homogeneous conditions)
k_t	transducer constant
ψ	near field correction factor
r	distance from transducer face
C	mass concentration
α_w	attenuation of water
α_{sh}	attenuation of suspended particles (under homogeneous conditions)

Measurement principle

UNIVERSITY OF LEEDS

$$\frac{\partial G}{\partial r} = -2(\alpha_w + \alpha_s)$$

$$\alpha_w = 0.05641 f^2 \mathrm{e}^{\left(-\frac{T}{27}\right)} \qquad \alpha_s = \xi_h C$$

~~k_s~~	~~particle species backscatter co-efficient~~
~~k_t~~	~~transducer constant~~
ψ	near field correction factor
r	distance from transducer face
C	mass concentration
α_w	attenuation of water
α_s	attenuation of suspended particles

H. Rice *et al*, “Measuring particle concentration in multiphase pipe flow using acoustic backscatter: Generalization of the dual-frequency inversion method,” *J. Acoust. Soc. Am.*, vol. 136, no. 1, pp. 156-169, 2014.

Acoustics Calibration

Instrument in prototype enclosure

UNIVERSITY OF LEEDS

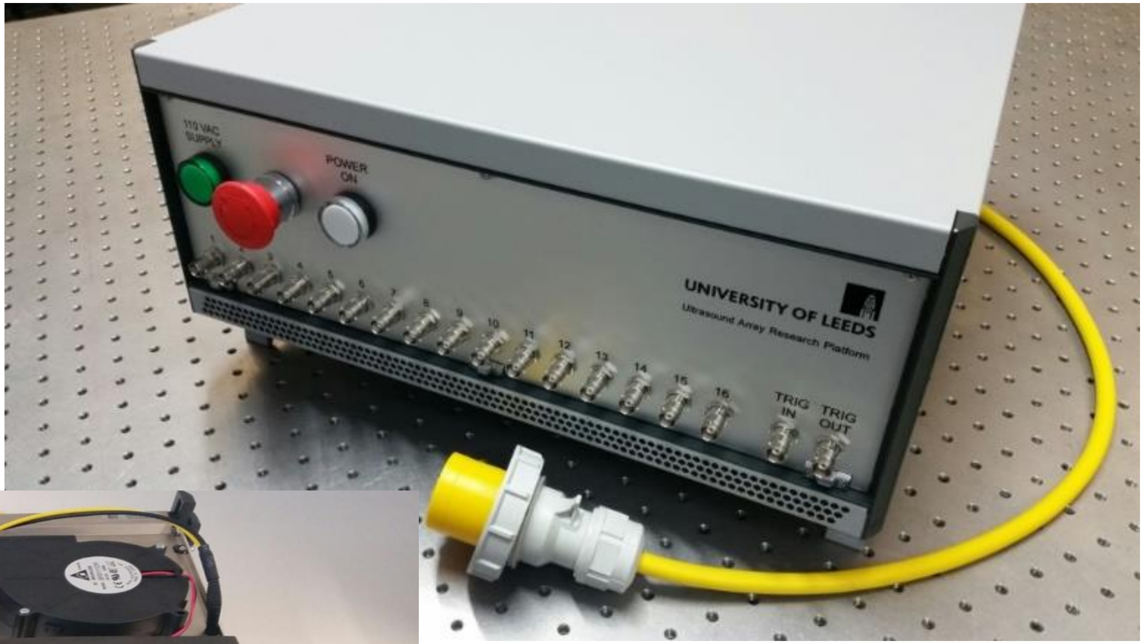

Acoustics calibration

UNIVERSITY OF LEEDS

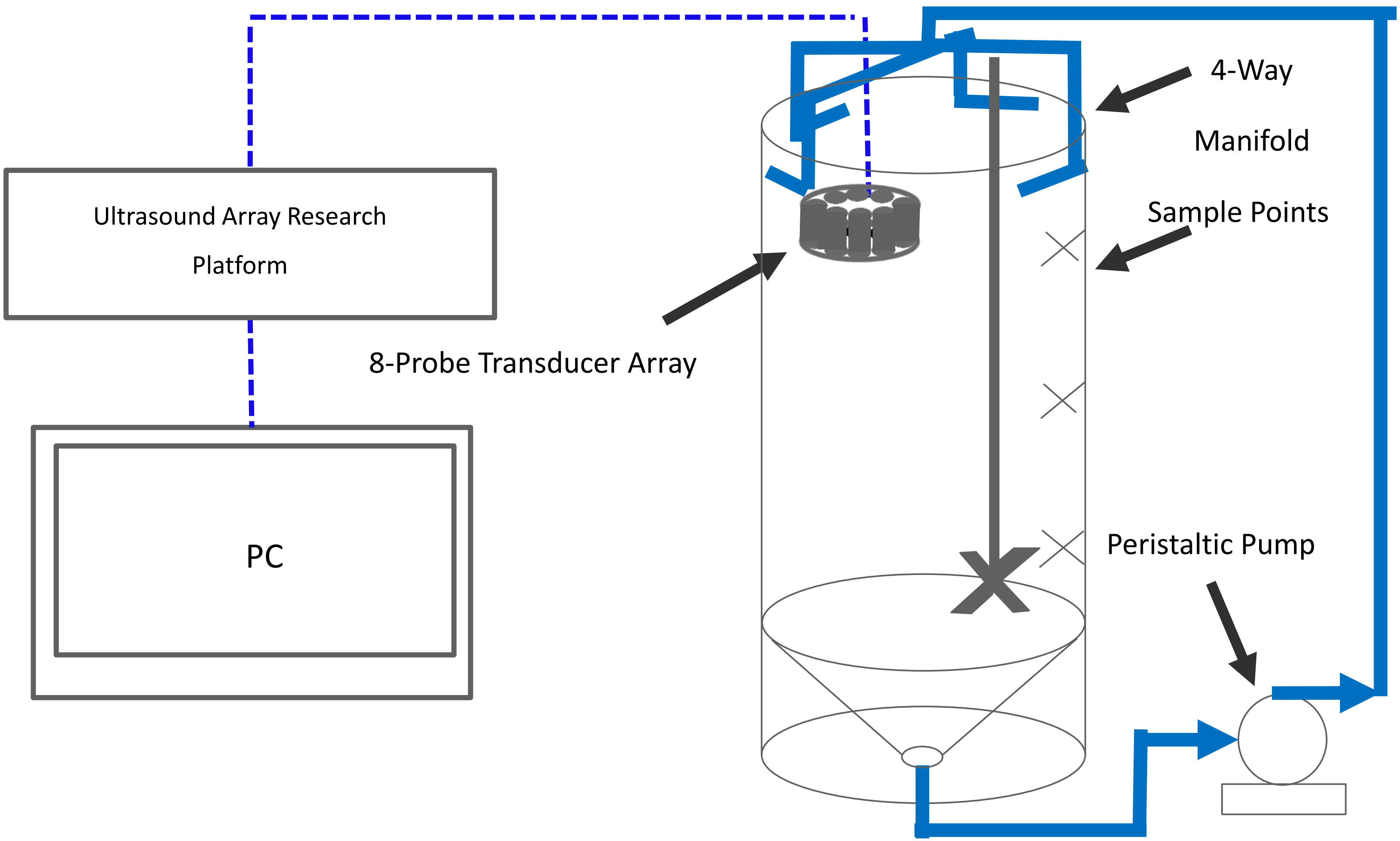

Calibration Data

UNIVERSITY OF LEEDS

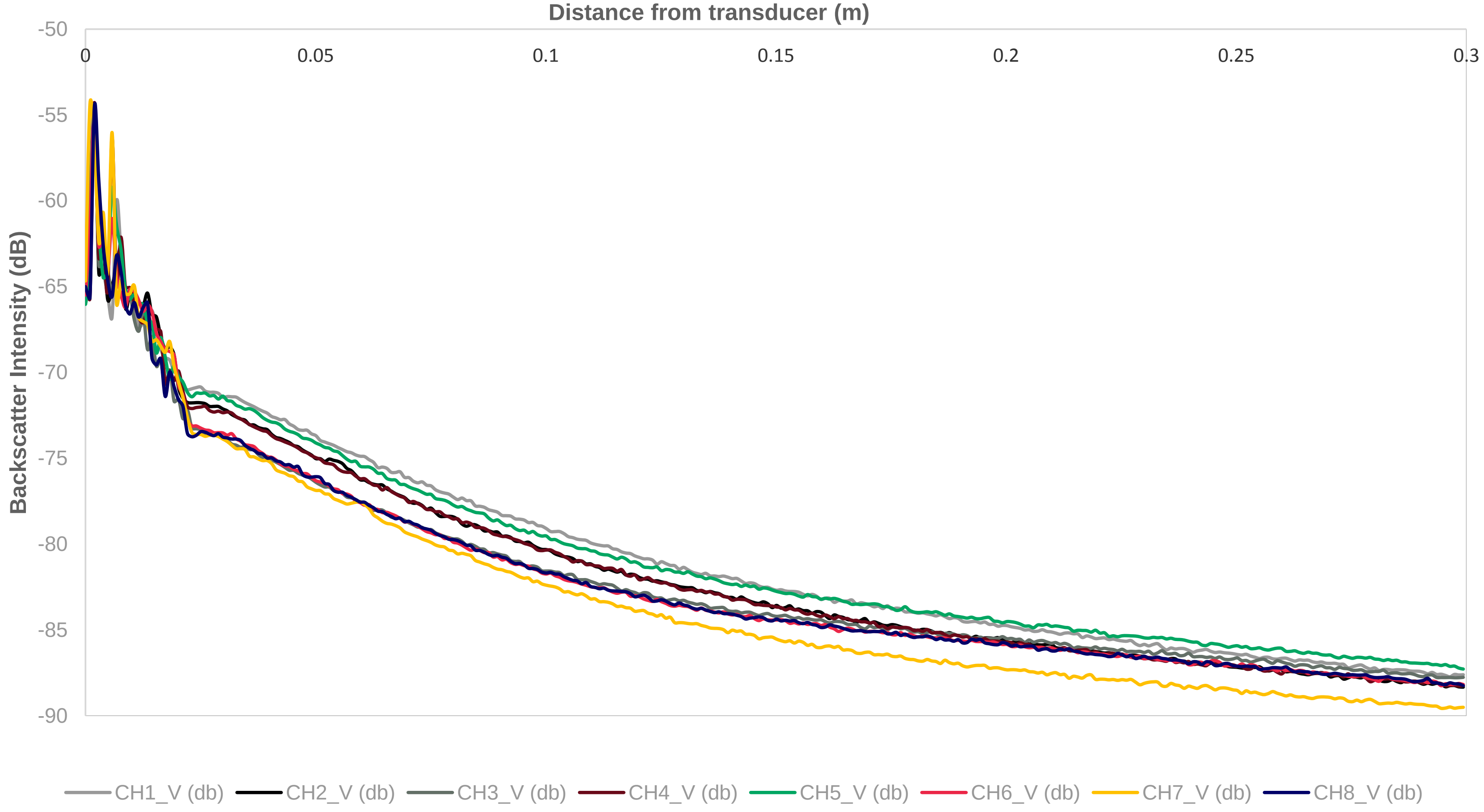

Calibration Data

UNIVERSITY OF LEEDS

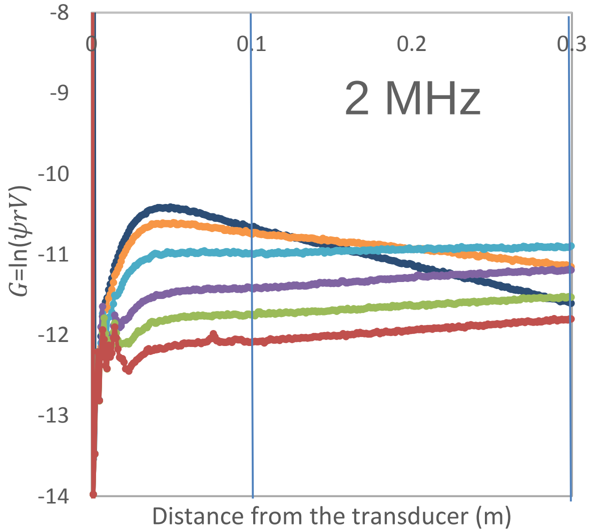

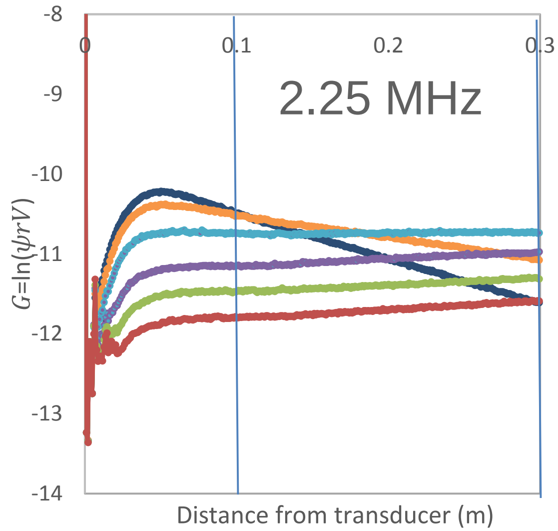

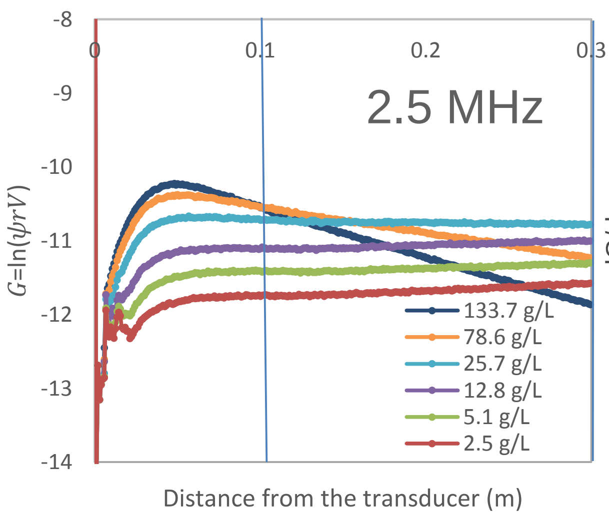

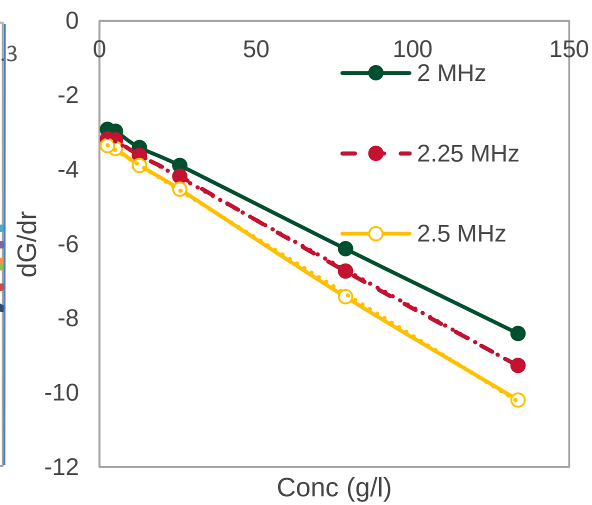

$$\frac{\partial G}{\partial r} = -2(\alpha_w + \alpha_s)$$

$$\frac{\partial G}{\partial r} = -2(\alpha_w + \xi_h C)$$

$$\xi_h = -\frac{\frac{1}{2}\left(\frac{\partial G}{\partial r}\right)}{\partial C}$$

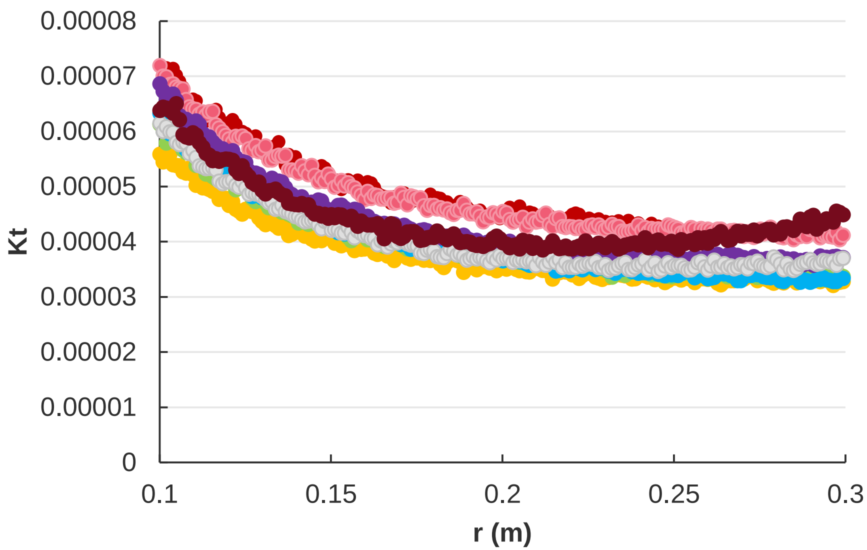
0.00008
0.00007
0.00006
0.00005
0.00004
0.00003
0.00002
0.00001
0
Kt
0.1
0.15
0.2
0.25
0.3
r (m)

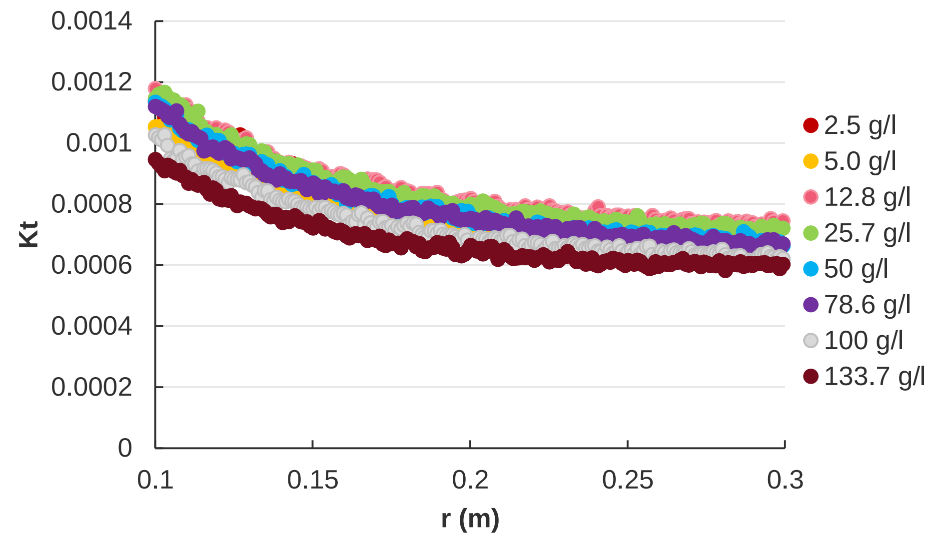
0.0014
0.0012
0.001
0.0008
0.0006
0.0004
0.0002
0
Kt
0.1
0.15
0.2
0.25
0.3
r (m)
2.5 g/l
5.0 g/l
12.8 g/l
25.7 g/l
50 g/l
78.6 g/l
100 g/l
133.7 g/l

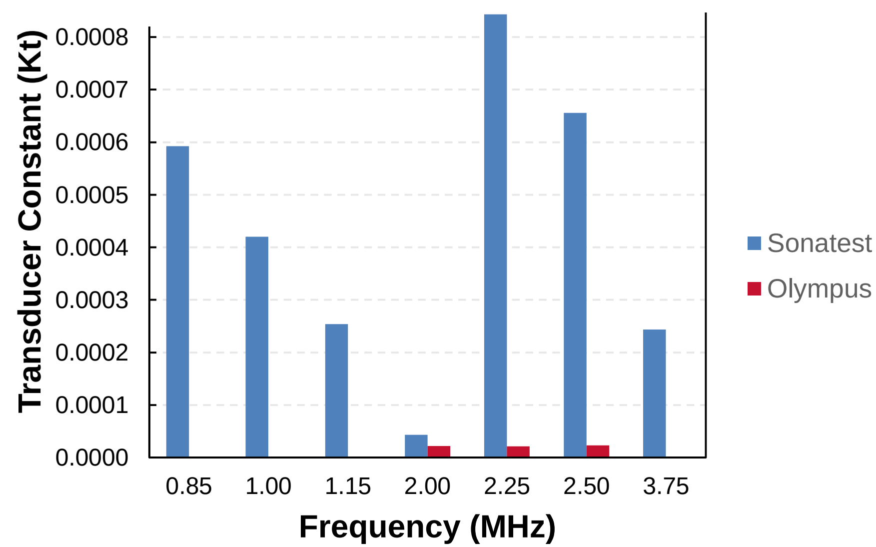
Transducer Constant (Kt)
0.0008
0.0007
0.0006
0.0005
0.0004
0.0003
0.0002
0.0001
0.0000
0.85
1.00
1.15
2.00
2.25
2.50
3.75
Frequency (MHz)
Sonatest
Olympus

Calibration Data

UNIVERSITY OF LEEDS

$$k = \frac{2\pi}{\lambda}$$

$$\chi = \frac{4\, a_s \rho_s\, \xi}{3}$$

k = Wavenumber (m^{-1})
λ = Wavelength (m)
χ = Scattering cross section (m^2)
ρ_s = Sediment particle density (kgm^{-3})
a_s = Particle diameter (m)

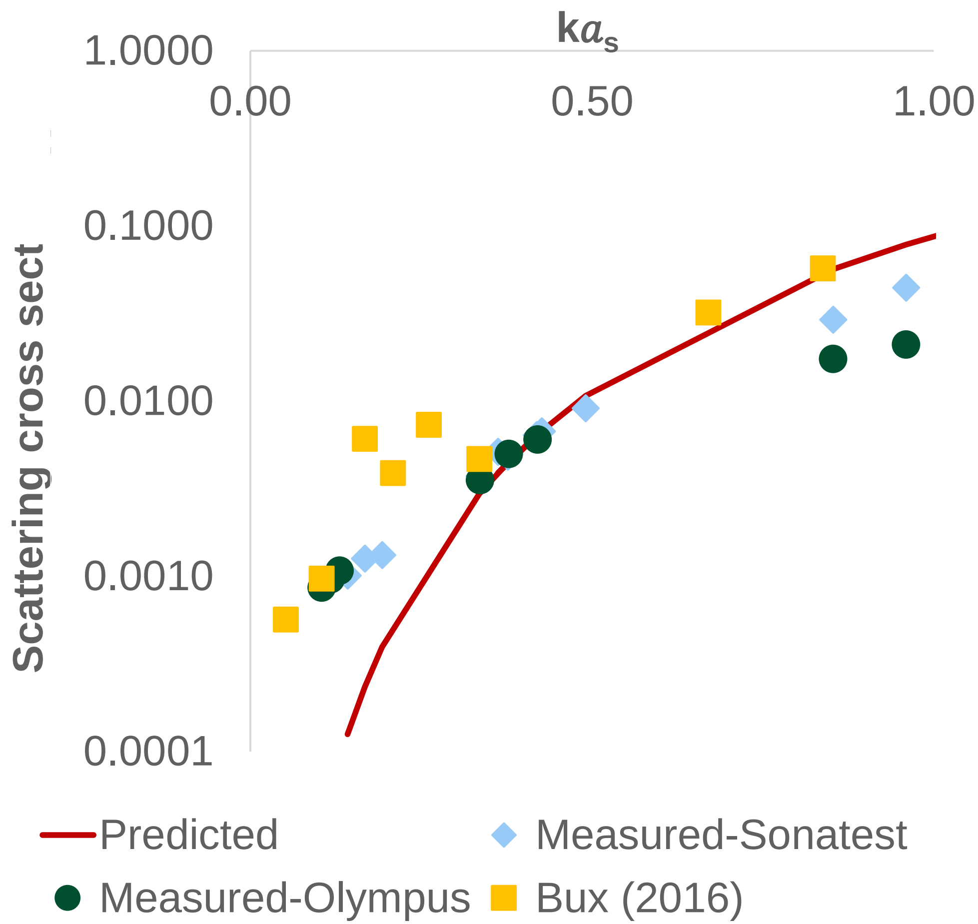

New Sampling System

UNIVERSITY OF LEEDS

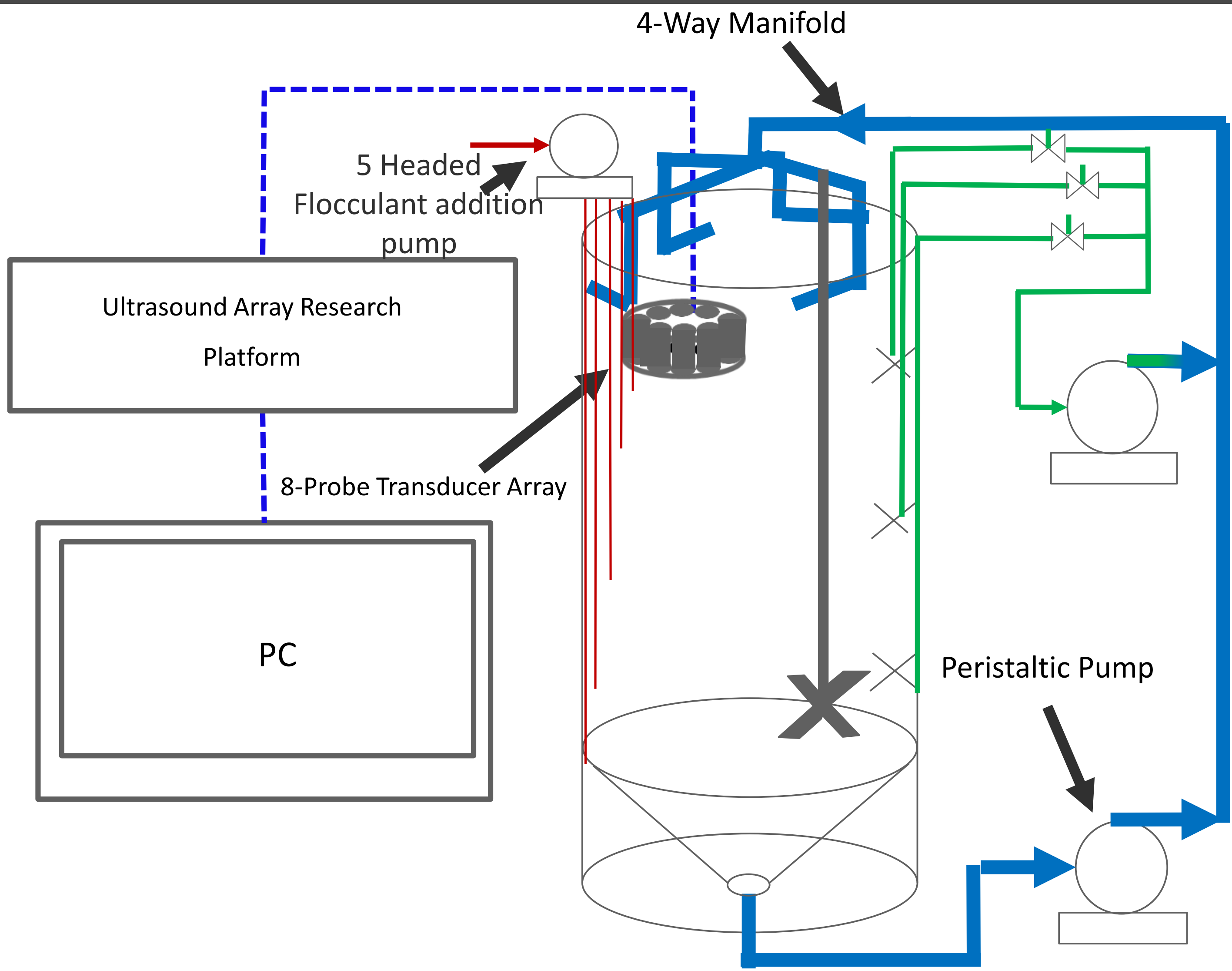

Future Work

UNIVERSITY OF LEEDS

- Collect large angle light scattering (LALS) for flocs using Saturn Digisizer
- Set up new sampling/ flocculant delivery system

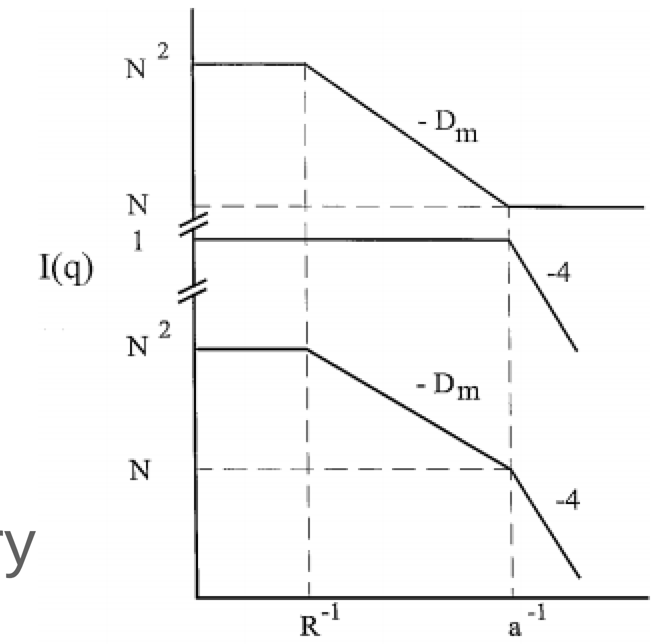

C.M. Sorensen, “Light Scattering by Fractal Aggregates: A Review,” Aerosol Science and Technology, vol. 35, pp. 648-687, 2001.

Future Work

UNIVERSITY OF LEEDS

- Synthesise latex particles using XME rig and collect acoustic and size data (FBRM, mastersizer, digisizer) to compare to data collected by Bux (2016)

- Repeat previous flocculation experiments and document size change over time using FBRM so that flocs may be characterised acoustically according to size and structure